JOURNAL OF GEOPHYSICAL RESEARCH, VOL. 104, NO. D21, PAGES 26,687–26,703, NOVEMBER 20, 1999

# Comparison of modeled and observed values of $NO_2$ and $JNO_2$ during the Photochemistry of Ozone Loss in the Arctic Region in Summer (POLARIS) mission

L. A. Del Negro,[1,2,3] D. W. Fahey,[1] R. S. Gao,[1,2] S. G. Donnelly,[1,2] E. R. Keim,[4] J. A. Neuman,[1,2] R. C. Cohen,[5] K. K. Perkins,[6] L. C. Koch,[5] R. J. Salawitch,[7] S. A. Lloyd,[8] M. H. Proffitt,[1,2] J. J. Margitan,[7] R. M. Stimpfle,[6] G. P. Bonne,[6] P. B. Voss,[6] P. O. Wennberg,[9] C. T. McElroy,[10] W. H. Swartz,[8,11] T. L. Kusterer,[8] D. E. Anderson,[8] L. R. Lait,[12] and T. P. Bui[13]

**Abstract.** Stratospheric measurements of NO, $NO_2$, $O_3$, ClO, and $HO_2$ were made during spring, early summer, and late summer in the Arctic region during 1997 as part of the Photochemistry of Ozone Loss in the Arctic Region in Summer (POLARIS) field campaign. In the sunlit atmosphere, $NO_2$ and NO are in steady state through $NO_2$ photolysis and reactions involving $O_3$, ClO, BrO, and $HO_2$. By combining observations of $O_3$, ClO, and $HO_2$, observed and modeled values of the $NO_2$ photolysis rate coefficient ($J_{NO_2}$), and model estimates of BrO, several comparisons are made between steady state and measured values of both $NO_2$ and $J_{NO_2}$. An apparent seasonal dependence in discrepancies between calculated and measured values was found; however, a source for this dependence could not be identified. Overall, the mean linear fits in the various comparisons show agreement within 19%, well within the combined uncertainties (±50 to 70%). These results suggest that photochemistry controlling the $NO_2$/NO abundance ratio is well represented throughout much of the sunlit lower stratosphere. A reduction in the uncertainty of laboratory determinations of the rate coefficient of $NO + O_3 \rightarrow NO_2 + O_2$ would aid future analyses of these or similar atmospheric observations.

## 1. Introduction

With mixing ratios in the parts per trillion (pptv) to parts per billion (ppbv) range in the lower stratosphere, hydrogen, nitrogen, and halogen radicals ($HO_x$ = OH + $HO_2$; $NO_x$ = NO + $NO_2$; $ClO_x$ = Cl + ClO; $BrO_x$ = Br + BrO) play important roles in the destruction of stratospheric ozone ($O_3$) through their respective catalytic cycles. Although the net contribution to $O_3$ loss from the $HO_x$, $ClO_x$, and $BrO_x$ catalytic cycles generally exceeds that of $NO_x$ in the lower stratosphere at midlatitudes [*Wennberg et al.*, 1994], $NO_x$ plays a significant role in moderating $O_3$ destruction by controlling the partitioning between the hydroxy radical (OH) and the hydroperoxy radical ($HO_2$) and between chlorine monoxide (ClO) and chlorine nitrate ($ClONO_2$) in most regions of the atmosphere.

In the Photochemistry of Ozone Loss in the Arctic Region in Summer (POLARIS) mission, observations of $NO_x$, $NO_y$ (= NO + $NO_2$ + $NO_3$ + $N_2O_5$ + $ClONO_2$ + $HNO_3$ + HONO + $HO_2NO_2$ + $BrONO_2$. . .), and a variety of other reactive and long-lived species were obtained in the summer polar stratosphere. The observations considered here were made with instruments on board the NASA ER-2 high-altitude aircraft. POLARIS took place between April and September of 1997, with the majority of ER-2 flights originating from Fort Wainwright in Fairbanks, Alaska (65°N, 147°W). During summer in the Arctic lower stratosphere, mixing ratios of $NO_x$ (shaded area of Figure 1) are enhanced relative to total $NO_y$ and other radical species. During periods of continuous solar illumination, the rapid photolysis of nitrogen trioxide ($NO_3$, nitrate radical) prevents formation of dinitrogen pentoxide ($N_2O_5$), thereby shutting down one of the major pathways for converting $NO_x$ to nitric acid ($HNO_3$). Long hours of sunlight also increase the role of other photolytic pathways within the $NO_y$ reservoir, converting higher oxides of nitrogen to nitrogen dioxide ($NO_2$), as indicated by the dashed arrows in Figure 1. These changes in photochemical conditions increase the local contribution of $NO_x$ to $O_3$ loss rates

[1]Aeronomy Laboratory, National Oceanic and Atmospheric Administration, Boulder, Colorado.
[2]Cooperative Institute for Research in Environmental Sciences, University of Colorado, Boulder
[3]Department of Chemistry and Biochemistry, University of Colorado, Boulder.
[4]Space and Environmental Technology Center, The Aerospace Corporation, Los Angeles, California.
[5]Department of Chemistry, University of California, Berkeley.
[6]Department of Chemistry, Harvard University, Cambridge, Massachusetts.
[7]Jet Propulsion Laboratory, California Institute of Technology, Pasadena
[8]Johns Hopkins University Applied Physics Laboratory, Laurel, Maryland.
[9]Division of Geological and Planetary Sciences, California Institute of Technology, Pasadena.
[10]Atmospheric Environment Service, Environment Canada, Downsview, Ontario, Canada.
[11]Department of Chemistry and Biochemistry, University of Maryland, College Park.
[12]NASA Goddard Space Flight Center, Greenbelt, Maryland.
[13]NASA Ames Research Center, Moffett Field, California



Paper number 1999JD900246.
0148-0227/99/1999JD900246$09.00

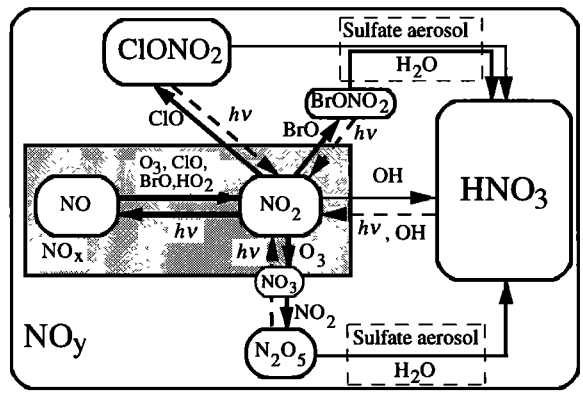


**Figure 1.** Diagram denoting the principal species of the $NO_y$ reservoir and reaction pathways relevant to the lower stratosphere. Larger boxes and thicker arrows indicate a greater abundance and larger reaction rate, respectively, but are not necessarily to scale. Photolysis is designated by dashed arrows and the label hν.

[*Randeniya et al.*, 1997; *Bruhl et al.*, 1998]. Studies of $NO_x/NO_y$ ratios for POLARIS have shown that models using reaction rate coefficients from *DeMore et al.* [1997] significantly underestimate this ratio [*Gao et al.*, 1999; *Drdla et al.*, this issue; *Osterman et al.*, 1999]. Though a variety of models (semi-empirical, diurnal photochemical steady state, and trajectory models) have been used in these analyses, all include the same reactions that define the steady state relationship between nitric oxide (NO) and $NO_2$, as shown in the shaded region in Figure 1.

NO and $NO_2$ interconvert through the following reactions:

(R1) $NO_2 + h\nu \rightarrow NO + O$

(R2) $NO + O_3 \rightarrow NO_2 + O_2$

(R3) $NO + ClO \rightarrow NO_2 + Cl$

(R4) $NO + BrO \rightarrow NO_2 + Br$

(R5) $NO + HO_2 \rightarrow NO_2 + OH$

Owing to the short lifetime (~60-200 s) of $NO_2$ through reaction (R1) at 20 km [*DeMore et al.*, 1997], a nearly instantaneous photochemical steady state exists between NO and $NO_2$ for most daytime conditions in the lower stratosphere. Other reactions, such as those that interconvert $NO_2$ and $HNO_3$, $BrONO_2$, $ClONO_2$, and $N_2O_5$ (Figure 1), are orders of magnitude slower and do not participate in defining the steady state partitioning of NO and $NO_2$. This steady state can be used to estimate values of $NO_2$ from measurements of other species through the following expression:

$$[NO_2]_{ss} = \frac{\{k_2[O_3] + k_3[ClO] + k_4[BrO] + k_5[HO_2]\}[NO]}{J_{NO_2}} \quad (1a)$$

where $k_n$ represents the reaction rate coefficient for reaction (R$n$), $J_{NO_2}$ represents the photolysis rate coefficient for reaction (R1), and [X] represents the number density of species X. Because of the limited contribution of the ClO, BrO, and $HO_2$ terms in (1a), this expression is sometimes approximated as follows:

$$[NO_2]_{ss} = \frac{\{k_2[O_3] + k_3[ClO] + k_4[BrO]\}[NO]}{J_{NO_2}}, \quad (1b)$$

$$[NO_2]_{ss} = \frac{\{k_2[O_3] + k_3[ClO]\}[NO]}{J_{NO_2}}, \quad (1c)$$

or

$$[NO_2]_{ss} = \frac{k_2[O_3][NO]}{J_{NO_2}}. \quad (1d)$$

Some past evaluations of $[NO_2]_{ss}$ have used simultaneous in situ measurements of NO, $NO_2$, $O_3$, and ClO (equation (1c)) and calculated values of BrO (equation (1b)), covering regions from midlatitudes to Antarctic high latitudes. These studies have demonstrated that values of $[NO_2]_{ss}$ are larger than measured values of $NO_2$ by between 8% [*Gao et al.*, 1997] and 40% [*Jaeglé et al.*, 1994]. In contrast, observations of $NO_2$ made from the balloon-borne Jet Propulsion Laboratory MkIV Interferometer were larger than $NO_2$ values calculated with a photochemical model by up to 30% for altitudes less than 30 km [*Sen et al.*, 1998].

The steady state expression in equation (1a) can be rearranged to solve for $J_{NO_2}$ as

$$J_{NO_2,ss} = \frac{\{k_2[O_3] + k_3[ClO] + k_4[BrO] + k_5[HO_2]\}[NO]}{[NO_2]}, \quad (2)$$

where $J_{NO_2,ss}$ is defined as the value of $J_{NO_2}$ calculated from (2) using measured values of $NO_2$ and other species. Equations (1a) and (2) are mathematically related. Using equation (2), $J_{NO_2,ss}$ values are compared directly with values of $J_{NO_2}$ derived from radiation field models and from spectroradiometer observations.

In this study, comparisons will be made between measured values of $NO_2$ and values of $[NO_2]_{ss}$ calculated with equations (1a) – (1d). The contributions of the BrO, $HO_2$, and ClO terms to steady state production of $NO_2$ will be evaluated for each of the three POLARIS deployments. In addition, values of $J_{NO_2,ss}$ calculated according to equation (2) will be compared with values of $J_{NO_2}$ derived from spectroradiometer observations on the ER-2 and from radiation field models.

## 2. Measurements and Derived Quantities

Typical ER-2 flights during POLARIS ranged from 6-8 hours in length, during which the ER-2 cruised at an altitude of ~18-20 km (~65 mbar) in the lower stratosphere. The observations used in the current analysis were selected from the POLARIS data set for pressures between 50 and 100 mbar to remove measurement uncertainties associated with aircraft ascents and descents. A list of the POLARIS flights used here and the range of conditions encountered by the ER-2 is

given in Table 1. ER-2 instrument characteristics are given in Table 2.

### 2.1. NO and $NO_2$

Measurements of NO and $NO_2$ were provided by the National Oceanic and Atmospheric Administration (NOAA) Aeronomy Laboratory chemiluminescence detector. NO is detected using the chemiluminescent reaction with $O_3$. In a photolysis cell located upstream of the chemiluminescence reaction vessel, 30 to 50% of ambient $NO_2$ is converted into NO. A schematic of the photolysis system is shown in Figure 2, and operating characteristics and uncertainty terms are listed in Table 3. A combination of color-glass optical filters reduces the UV bandwidth from the broad band light that reaches the ambient sample and selectively photolyzes $NO_2$ [*Gao et al.*, 1997]. Fans provide cooling air from a duct along the aircraft skin to minimize heating of the ambient sample, the photolysis cell, and the filters.

When the shutter between the photolysis lamp and cell is open, the NO signal measured in the $NO_2$ channel is the sum of ambient NO ($NO_{amb}$) plus the fraction of ambient $NO_2$ ($NO_{2amb}$) converted to NO in the photolysis cell, or

$$NO_{meas} = NO_{amb} + \alpha NO_{2amb} \quad (3)$$

where $\alpha$ represents the conversion fraction. The value of $NO_{2amb}$ can be determined provided $NO_{amb}$ and $\alpha$ are known. $NO_{amb}$ is measured in the NO channel of the instrument and occasionally in the $NO_2$ channel when the shutter is closed. Provided there is good agreement between the NO and $NO_2$ channel measurements of $NO_{amb}$, values of $NO_{amb}$ from the NO channel are used to represent $NO_{amb}$ in the $NO_2$ channel of the instrument when the shutter is open. The value of $\alpha$ is

**Table 1.** POLARIS Flights and Conditions.

| Flight | Date[a] | Temperature, K | Latitude, °N | SZA, deg[b] | Solar Exposure[c] | $O_3$, ppmv | NO, ppbv | $NO_2$,[d] ppbv | $NO_y$ ppbv | SA[e] μm2 cm-3 |
|---|---|---|---|---|---|---|---|---|---|---|
| | | | | | *Deployment I* | | | | | |
| I-1 | April 22[f] | 195-211 | 14-37 | 10-72 | 0.55-0.61 | 0.2-2.6 | 0.2-0.8 | 0.1-0.6 | 0.7-7.8 | 1.3-4.0 |
| I-2 | April 24 | 210-227 | 37-66 | 41-54 | 0.53-0.65 | 0.5-3.2 | 0.2-0.6 | 0.1-0.9 | 1.6-10.0 | 0.8-2.3 |
| I-3 | April 26[f] | 214-229 | 66-90 | 58-77 | 0.58-0.80 | 1.3-3.4 | 0.1-1.0 | 0.3-1.6 | 4.1-12.0 | 0.7-2.4 |
| I-4 | April 30[g] | 225-230 | 64-65 | 72-101 | 0.59-0.71 | 1.0-2.7 | 0.1-0.2 | 0.3-0.6 | 3.4-8.7 | 1.2-2.2 |
| I-5 | May 2 | 226-231 | 66-71 | 55-66 | 0.67-0.92 | 1.1-3.1 | 0.2-0.6 | 0.3-1.1 | 3.5-8.7 | 0.9-2.3 |
| I-6 | May 6[f] | 226-234 | 65-79 | 53-63 | 0.75-1.00 | 1.0-3.3 | 0.2-0.7 | 0.3-1.3 | 3.5-10.8 | 0.9-2.3 |
| I-7 | May 9[g] | 227-229 | 64 -65 | 78-98 | 0.76-0.93 | 1.0-2.8 | 0.2-0.3 | 0.4-1.0 | 3.4-8.8 | 1.2-2.4 |
| I-8 | May 13 | 226-234 | 66-85 | 55-67 | 0.71-1.00 | 1.7-3.1 | 0.2-0.9 | 0.3-1.3 | 4.0-9.6 | 0.8-2.3 |
| mean | | 224 | 63 | 57 | 0.76 | 2.4 | 0.5 | 0.8 | 7.1 | 1.4 |
| | | | | | *Deployment II* | | | | | |
| II-1 | June 26 | 223-231 | 55-77 | 41-58 | 0.71-1.0 | 0.9-2.8 | 0.4-1.5 | 0.3-1.8 | 3.4-12.3 | 0.7-2.3 |
| II-2 | June 29 | 220-227 | 48-64 | 33-58 | 0.65-1.00 | 0.8-2.8 | 0.4-1.7 | 0.3-1.3 | 3.3-12.6 | 0.6-2.2 |
| II-3 | June 30[h] | 224-228 | 63-67 | 40-47 | 0.92-1.00 | 1.0-2.4 | 0.4-1.6 | 0.4-1.6 | 3.5-11.7 | 0.6-2.4 |
| II-4 | July 4 | 218-230 | 48-71 | 27-58 | 0.61-1.00 | 0.8-2.7 | 0.3-1.5 | 0.2-1.9 | 2.7-12.0 | 0 6-2.3 |
| II-5 | July 7[f] | 227-233 | 65-90 | 54-68 | 1.00 | 1.1-2.7 | 0.4-1.8 | 0.5-1.9 | 4.2-12.9 | 0.6-2.3 |
| II-6 | July 10 | 225-229 | 63-66 | 41-57 | 0.81-0.90 | 1.1-2.7 | 0.4-1.3 | 0.4-1.2 | 4.3-11.2 | - |
| mean | | 227 | 65 | 47 | 0.92 | 2.0 | 0.8 | 0.9 | 7.6 | 1.2 |
| | | | | | *Deployment III* | | | | | |
| III-1 | Sept. 8 | 220-228 | 65-86 | 67-101 | 0.58-1.00 | 0.7-2.7 | 0.2-0.8 | 0.2-1.0 | 2.8-10.6 | 0.7-2.3 |
| III-2 | Sept. 11[g] | 221-224 | 64-65 | 77-102 | 0.59-0.61 | 0.9-1.9 | 0.2-0 7 | 0.3-1.2 | 3.2-7.9 | 1.4-2.8 |
| III-3 | Sept. 14[h] | 217-221 | 64-65 | 66-102 | 0.51-0.57 | 0.6-2.0 | 0.1-0.5 | 0.3-0.7 | 2.6-8.2 | 1.1-2.4 |
| III-4 | Sept. 15[h] | 219-222 | 64-65 | 66-103 | 0.53-0.55 | 0.5-2.1 | 0.0-0.9 | 0.3-1.2 | 1.8-9.1 | 1.1-3.4 |
| III-5 | Sept. 18 | 219-227 | 66-87 | 73-99 | 0.55-0.88 | 0.7-2.7 | 0.1-0.6 | 0.2-0.8 | 2.5-10.9 | 0.7-2.6 |
| III-6 | Sept. 19 | 222-227 | 64-65 | 63-85 | 0.57-0.59 | 1.3-2.1 | 0.1-0.5 | 0.2-0.7 | 5.0-8.4 | 1.1-2.4 |
| III-7 | Sept. 21 | 200-224 | 23-62 | 35-74 | 0.51-0.59 | 0.2-2.2 | 0.1-0.8 | 0.1-0.5 | 0.7-8.9 | 1.0-6.0 |
| III-8 | Sept. 23 | 194-213 | -3-20 | 0-67 | 0.50-0.55 | 0.1-1.7 | 0.2-0.6 | 0.1-0.3 | 0.4-2.9 | - |
| mean | | 218 | 55 | 62 | 0.61 | 1.7 | 0.4 | 0.4 | 6.2 | 1.3 |

All data except SZA and solar exposure are provided by instruments in Table 2.

[a] All dates refer to 1997 flights; flight lengths range from 4 to 8 hours.

[b] Solar zenith angle.

[c] Average fractional solar exposure received by a sampled air parcel over the previous five days as described in Results and Discussion section.

[d] Measurements by Aeronomy Laboratory photolysis/chemiluminescence system.

[e] Aerosol surface area density.

[f] Indicates a flight that is not included in Figure 4 because $[NO_2]_{HU}$ data were unavailable.

[g] Indicates a sunrise or sunset flight for which a substantial fraction of the data (at SZAs > 85°) have been removed from the analysis and comparisons shown in Plates 3 and 4.

[h] Indicates a flight that is not included in Plates 3 and 4 because $HO_2$ data were unavailable.

**Table 2.** ER-2 Instrument Characteristics

| Species | Technique | Reference | Sample Period, s | Uncertainty ±1 σ |
|---|---|---|---|---|
| NO | chemiluminescence | *Fahey et al.* [1989] | 1 | ±6% + 4 pptv |
| $[NO_2]_{AL}$ | chemiluminescence | *Gao et al.* [1994,1997] | 1 | ±15-30% |
| $[NO_2]_{HU}$ | laser-induced fluorescence | K. K. Perkins et al. (manuscript in preparation, 1999a, b) | 10-20 | ±10% ± 50 pptv |
| $O_3$ | UV absorption | *Proffitt et al.* [1989] | 1 | ±5% |
| ClO | resonance fluorescence | *Brune et al.*[1989] | 35 | ±15% |
| $HO_2$ | laser-induced fluorescence | *Wennberg et al.* [1994,1995] | 2 | ±15% |
| $J_{NO_2}$ | spectroradiometer | *McElroy et al.* [1995] | 132 | ±15% |
| Pressure | aircraft probe | *Chan et al.* [1989] | 1 | ±0.25 mbar |
| Temperature | aircraft probe | *Chan et al.* [1989] | 1 | ±0 3 K |
| $N_2O$ | tunable diode laser absorption spectroscopy | *Loewenstein et al.* [1989] | 1 | ±2% |
| Surface area | optical particle counter | *Jonsson et al* [1995] | 30 | ±60% |

determined by adding $NO_2$ calibration gas to the ambient sample in flight. The $NO_2$ photolysis system has been used in previous campaigns with an estimated instrumental uncertainty range of 30 to 60% [*Gao et al.*, 1994, 1997]. $NO_2$ data used in the present analysis have an estimated instrumental uncertainty range from 10 to 30%. Characteristics of the system used during POLARIS, as well as the modifications to the instrument that resulted in this improved performance, are described briefly in the next sections.

**2.1.1. UV lamp evaluation.** The characteristics of the radiation reaching the cell from the photolysis lamp are shown in Figure 3. In addition to controlling the UV bandwidth reaching the photolysis cell, the color-glass filters also reduce the transmitted IR radiation, and therefore the resulting temperature of the photolysis cell and sample air. The filter configuration used in previous field campaigns consisted of a Pyrex® window, a 2-mm thick Schott UG-5 band-pass filter, and a 2-mm Schott WG-345 long-pass filter. The transmittance of each of these components is shown in Figure 3a. The addition of a 2-mm Schott WG-360 long-pass filter to the above configuration

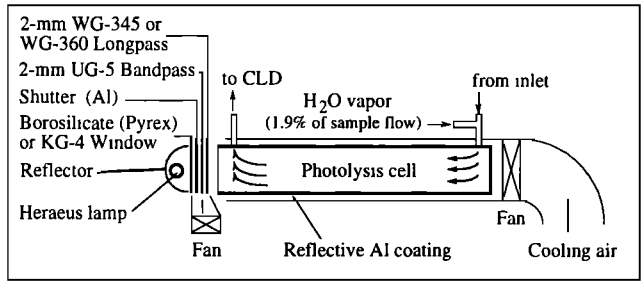


**Figure 2.** Schematic of the NOAA Aeronomy Laboratory $NO_2$ photolysis system on board the ER-2. The sample air is pulled through the inlet and photolysis cell prior to NO detection in the chemiluminescence detector. The cylindrical cell is approximately 25 cm long with a diameter of approximately 5 cm.

further limited transmittance of wavelengths in the 330 to 380 nm range. However, the four-filter configuration was found to severely limit the fraction of $NO_2$ converted to NO without providing any significant advantages. In another test, a 2-mm Schott KG-4 color-glass filter was used to replace the Pyrex® window in the configuration. As shown in Figure 3a, the KG-4 filter provides lower transmittance than Pyrex® for wavelengths from 260 to 600 nm. Although not shown in Figure 3a, the KG-4 also provides significant reductions in the transmittance of wavelengths up to 5000 nm.

Two filter configurations were used during the POLARIS campaign. The initial configuration (KG-4, UG-5, and WG-360) was used for flights during Deployment I, while the final configuration (Pyrex®, UG-5, and WG-345) was used for all flights in Deployments II and III. The product of the transmittance of the filter set with the relative intensity of the Heraeus lamp, defined as the relative transmittance, is shown for both configurations in Figure 3b. In the initial configuration (short dashes), wavelengths from 345 to 410 nm were transmitted into the photolysis cell with a relative transmittance of approximately 1 or better. The peak in this curve is 43, which occurs at a wavelength of 370 nm. The corresponding value of α for this configuration was 0.36 to 0.38. In the final configuration (long dashes), the UV intensity reaching the cell was increased, leading to a peak value of 63 for the relative transmittance and giving α ranging from 0.48 to 0.56. The larger range in α for the final configuration is likely due to photoaging of the color-glass filters. Values of α began at 0.56 with new filters and dropped gradually with exposure time. Although the $HNO_3$ photolysis rate was increased in the final configuration due to the increased transmittance of UV radiation, laboratory tests have indicated an upper limit of 0.002 for the conversion fraction of $HNO_3$ to $NO_2$. This upper limit corresponds to a maximum uncertainty in $NO_2$ mixing ratios at cruise altitudes of ~4% for POLARIS flights.

**2.1.2. $NO_{amb}$ loss and the addition of water vapor.** In previous campaigns discrepancies in the value of $NO_{amb}$ were found between the NO and $NO_2$ channels of

**Table 3.** NOAA AL $NO_2$ Photolysis System Operational Characteristics

| | Average Value | Range Over Useable POLARIS Flights |
|---|---|---|
| Parameter | | |
| Cell pressure | 60 mbar | 59 - 62 mbar |
| Cell temperature (external) | 12.8°C | -5 - 28°C[a] |
| Sample air temperature | 12°C | -10 - 22°C[a] |
| Cell volume | 500 $cm^3$ | - |
| Cell sample flow | 968 sccm[b] | 965 - 971 sccm[b] |
| Residence time | 1.2 seconds | 1.1 - 1.3 seconds |
| $NO_2$ artifact in ZAir[c] | 47 pptv[d] | 20 - 76 pptv[d] |
| $NO_2$ sensitivity | 4.8 cps/pptv[e,f] | 4 7 - 5 1 cps/pptv[e,f] |
| | 6.5 cps/pptv[e,g] | 6.0 - 7.3 cps/pptv[e,g] |
| $NO_2$ conversion fraction | 0.37[f] | 0.36 - 0.38[f] |
| | 0.52[g] | 0.48 - 0.56[g] |
| NO sensitivity | 12 3 cps/pptv[e] | 12.1 - 12.9 cps/pptv[e] |
| $H_2O$ mixing ratio in sample line | 1.8% | ± 0.1% |
| $HNO_3$ conversion fraction | - | <0.2%[h] |
| Measurement Duty Cycle[i] | 65% | 55 - 68% |
| Uncertainty Term | | |
| Uncertainty in background | 3.1% | 0.8 - 27% |
| Uncertainty due to $NO_{amb}$ | 7.9% | 0.7 - 33%[j] |
| Uncertainty due to (R2) in sample line[k] | 1 9% | 0.8 - 7.7% |
| Uncertainty due to $HNO_3$ photolysis | 2.2% | 1.1 - 3.8% |
| Uncertainty due to absolute calibration | 6% | - |

[a] Varied with stratospheric ambient temperature.
[b] Here sccm, standard cubic centimeters per minute. Calibrated before and after each deployment.
[c] ZAir (or zero air) is synthetic air.
[d] Dependent on ambient signal, frequency of cell washing, etc.
[e] Here cps/pptv, counts per second per parts per trillion.
[f] Initial filter configuration.
[g] Final filter configuration.
[h] Upper limit. Laboratory tests at limit of detection.
[i] Percentage of time spent in ambient air measure mode (not zero or calibration).
[j] Although discrepancies between channels were less than 10% in all cases, the corresponding uncertainty in the $NO_2$ mixing ratio is a function of the ambient $NO_2$/NO ratio.
[k] Calculated for both NO and $NO_2$ channels.

the instrument. These discrepancies added a relatively large uncertainty to measured $NO_2$ mixing ratios and therefore were a primary focus for improving instrument performance. The discrepancy was determined to be due to a loss of $NO_{amb}$ in the $NO_2$ channel of the instrument when the cell was exposed to the photolysis lamp. This loss was diagnosed from the transient behavior of the $NO_{amb}$ signal after the shutter was closed and by comparison to the NO channel signal. When the shutter was closed, initial values of $NO_{amb}$ were as much as 50% less than values obtained in the NO channel of the instrument. After a period of 100 to 300 s during which the $NO_{amb}$ signal in the $NO_2$ channel rose dramatically, the $NO_{amb}$ signal returned to stable values equivalent to those in the NO channel of the instrument. This behavior indicated that little or no loss of $NO_{amb}$ was taking place in the dark photolysis cell. Therefore the loss process was associated with the photolytic radiation reaching the cell. In addition, because the residence time of ambient air in the photolysis cell is ~1.2 s, the relatively long time required for recovery of the $NO_{amb}$ signal indicated that the loss process most likely involved a surface reaction on the wall of the photolysis cell.

As noted above, 1-s sample values of $NO_{amb}$ from the NO channel are used in the calculation of $NO_2$ mixing ratios. Because $\alpha$ ranges from 0.3 to 0.5, differences in the response to $NO_{amb}$ between the NO and $NO_2$ channels, and the associated uncertainties, are magnified by factors of 2 to 3 in the calculated $NO_2$ mixing ratio. In the case of the discrepancy described above, values of $NO_{amb}$ from the NO channel (or from the shutter-closed $NO_2$ channel once the signal had stabilized) were not representative of the actual $NO_{amb}$ response in the $NO_2$ channel when the shutter was open. When low initial values of $NO_{amb}$ in the $NO_2$ channel found after the shutter was closed were used to estimate the actual response to $NO_{amb}$, these estimates were often inadequate, frequently generating negative mixing ratios for $NO_2$, and always adding large uncertainties to reported $NO_2$ mixing ratios.

In an attempt to correct this bias between the shutter-open and shutter-closed modes of the $NO_2$ channel, the

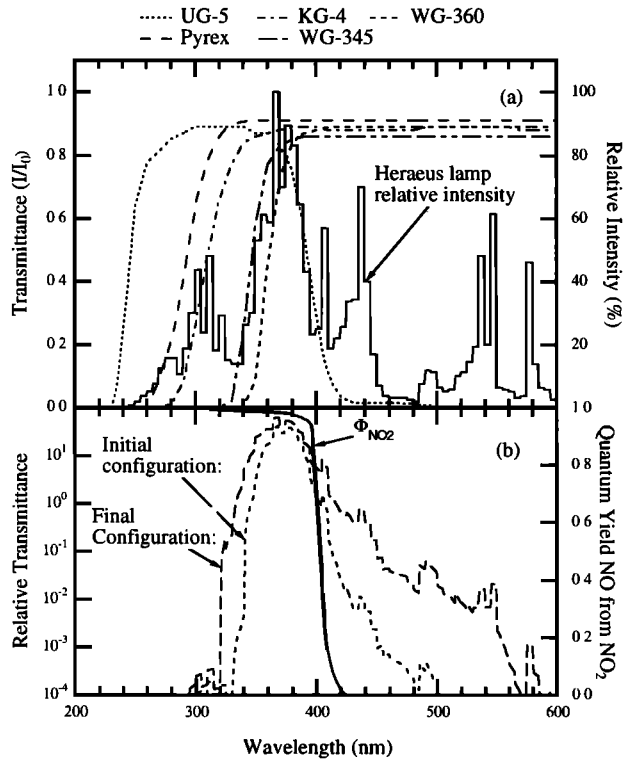


**Figure 3.** Characteristics of radiation entering the photolysis cell in the $NO_2$ channel. (a) Transmittance as a function of wavelength for various optical filters and the relative intensity of the Heraeus lamp output (*courtesy of Corning Incorporated, Schott Glass Technologies Incorporated, and Heraeus Amersil Incorporated*). (b) Relative transmittance (defined as the product of the lamp relative intensity and the filter set transmittance) for the two sets of filters used during the POLARIS field campaign as well as the photolysis quantum yield of NO from $NO_2$ ($\Phi_{NO_2}$) in this wavelength region [*DeMore et al.*, 1997]. The initial configuration consists of the combination of KG-4, UG-5, and WG-360 filters, while the final configuration was composed of Pyrex®, UG-5, and WG-345 filters (see Figure 2).

photolysis cell was tested in the laboratory to characterize the influence of UV bandwidth, sample temperature, reactions with ambient levels of $O_3$, and artifacts due to low-level $HNO_3$ photolysis. Despite the variety of tests performed, the loss of $NO_{amb}$ seen in flight could not be reproduced in the laboratory. In flight tests of the photolysis system before POLARIS in July, August, and December of 1996, loss of $NO_{amb}$ was found for each filter configuration discussed in the previous section. However, evidence of NO loss appeared only in the stratosphere and not in tropospheric flight legs of the ER-2. The differences suggested that an atmospheric constituent present with different abundances in the stratosphere than in the troposphere might be the cause. $H_2O$ was a good candidate because it has a large gradient across the tropopause. Thus, the addition of water vapor to the sample flow upstream of the photolysis cell in flight was checked and found to significantly reduce the loss of NO within the cell during flights in the stratosphere. Specifically, the addition of approximately 2% $H_2O$ by volume to the sample flow has been shown to effectively suppress the $NO_{amb}$ loss process without significantly reducing the sensitivity to $NO_2$ or NO. Although the specific role of $H_2O$ vapor in reducing the loss of NO is not known, $H_2O$ suppression of surface processes has a precedent in other atmospheric measurements. For example, $H_2O$ vapor is used to reduce noise in the reaction vessel of chemiluminescence detectors [*Drummond et al.*, 1985], and whole air samples are often taken in $H_2O$-passivated cans to prevent loss of more reactive species [*Heidt*, 1978]. All POLARIS flights included $H_2O$ addition to the sample flow, significantly lowering the bias between shutter-open and shutter-closed modes in the $NO_2$ channel.

**2.1.3. $NO_2$ Uncertainties.** Small differences in the measurement of $NO_{amb}$ between the NO and $NO_2$ channels of the instrument remained during POLARIS but did not have a consistent bias and were much smaller than the 50% differences described above. Average differences were less than ± 4%, with those in some isolated flight segments as high as 10%. The reduction in $NO_{amb}$ losses has significantly reduced the total uncertainty in the $NO_2$ measurement.

The total systematic uncertainty in the $NO_2$ mixing ratio has five components: background subtraction [*Gao et al.*, 1994], subtraction of $NO_{amb}$, reaction (R2) occurring in the temperature and pressure conditions of the sample line and photolysis cell, $HNO_3$ photolysis in the cell, and the absolute uncertainty associated with the concentration and delivery of the NO and $NO_2$ calibration gases. Thermal decomposition of $NO_y$ species in the photolysis cell can lead to interferences in the $NO_2$ measurement if the pressure or temperature in the cell is too high. Previous evaluations of $N_2O_5$, $HO_2NO_2$, and $ClONO_2$ in the laboratory have demonstrated the conditions under which such reactions may be a significant interference [*Gao et al.*, 1994]. Similarly, interference due to photodissociation of $NO_y$ species other than $HNO_3$, such as $ClONO_2$, $N_2O_5$, and $HO_2NO_2$, is expected to be less than 5% for conditions in the lower stratosphere [*Gao et al.*, 1994; *DeMore et al.*, 1997]. No evidence of these reactive or photolytic interferences was found during the POLARIS campaign. The uncertainty in $NO_2$ due to photolysis of $HNO_3$ is a function of the $NO_2/HNO_3$ ratio. As a result, although the upper limit of this uncertainty was 4% for POLARIS, it may increase in future field campaigns if the value of the ratio is significantly lower than that for POLARIS. The contribution of each uncertainty listed above is given in Table 3 as a percentage of the calculated $NO_2$ mixing ratio. For a given flight, the estimated average uncertainty in $NO_2$ mixing ratios at cruise altitudes ranged from 10 to 21%, with larger values at higher pressures. No values with uncertainties larger than 30% are included in the present study.

## 2.2. Additional Measurements

An additional measurement of $NO_2$ was provided during POLARIS by the new Harvard University laser-induced fluorescence (LIF) detector for $NO_2$ ($[NO_2]_{HU}$) [K. K. Perkins

et al., manuscript in preparation, 1999a]. Intercomparisons of measurements of $NO_2$ by the two systems show favorable results [K. K. Perkins et al., manuscript in preparation, 1999b]. For example, a comparison of the $NO_2$ mixing ratios for all POLARIS flights on which there were coincident measurements (see Table 1) is shown in Figure 4. The average difference between the two instruments is approximately 6%, a value well within the uncertainties of the individual measurements (see Table 2). The scatter in the data is likely due to the combination of instrument precision and atmospheric variability. Although the NOAA $NO_2$ ($[NO_2]_{AL}$) values are used in all of the analyses presented here, the use of $[NO_2]_{HU}$ measurements would lead to similar conclusions.

Since measurements of BrO were unavailable during the POLARIS campaign, values were obtained from the Jet Propulsion Laboratory (JPL) full-diurnal photochemical steady state (PSS) model that was run for points along each ER-2 flight track during POLARIS [*Salawitch et al.*, 1994a, b]. The PSS model includes 35 reactive species and approximately 220 chemical reactions. The model assumes that each species reaches a balance between production and loss over 24 hours for the temperature, pressure, and latitude at which an air parcel was sampled. Calculated concentrations of radical species were constrained by ER-2 measurements of pressure, temperature, aerosol surface area, long-lived precursors of free radicals (e.g., $H_2O$, $CH_4$, $NO_y$, $Cl_y$, $Br_y$ etc.), total column ozone as well as the ozone column above the ER-2 aircraft, and planetary albedo. The abundance of BrO was specified based on its correlation with CFC-11 [*Wamsley et al.*, 1998]. For the values of BrO used here, the model was constrained by NO rather than $NO_y$ and used reaction rates and absorption cross sections from *DeMore et al.* [1997], except for the rates of $OH + NO_2 + M$ [*Dransfield et al.*, 1999], $OH + HNO_3$ [*Brown et al.*, 1999], and a speculative $HO_x$ source discussed by *Wennberg et al.* [1999]. This model configuration was chosen for its improved ability to simulate observations of both $NO_x$ [*Gao et al.*, 1999] and $HO_x$ [*Wennberg et al.*, 1999], especially at high solar zenith angles (SZAs).

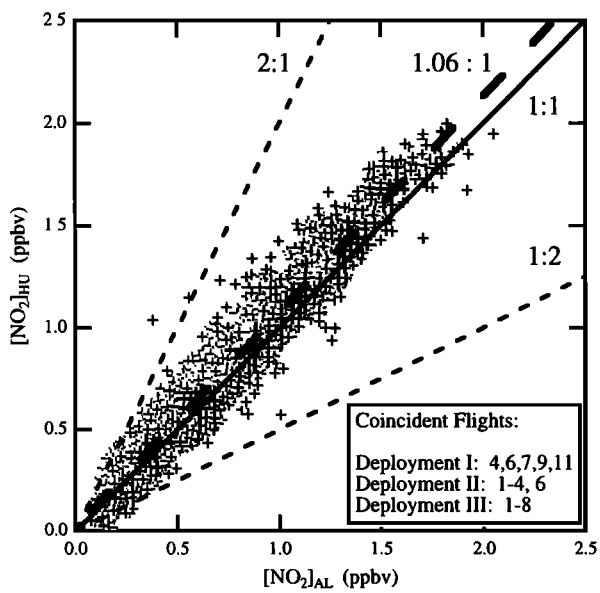


**Figure 4.** Comparison of all simultaneous $NO_2$ observations made by the NOAA Aeronomy Laboratory photolysis/chemiluminescence technique ($[NO_2]_{AL}$) and the Harvard University laser-induced fluorescence technique ($[NO_2]_{HU}$). $[NO_2]_{AL}$ data are 10 s averages of 1-s raw data; $[NO_2]_{HU}$ data are reported every 10 s. The solid line represents the 1:1 line; short-dashed lines represent the 2:1 and 1:2 lines. The best fit through the data (when forced through the origin) has a slope of 1.06 (long-dashed line).

A summary of other measurements used in this analysis is given in Table 2. Pressure, temperature, and other meteorological and positional data were collected by the NASA Ames micrometeorological measurement system (MMS) on board the ER-2.

### 2.3. $J_{NO_2}$ Values

Spectrally resolved solar actinic flux was measured by the Composition and Photodissociative Flux Measurement (CPFM) instrument on board the ER-2 [*McElroy*, 1995; *McElroy et al.*, 1995]. Using these flux data, the values of $J_{NO_2}$ and other photodissociation rates were derived. CPFM values of $J_{NO_2}$ (denoted $J_{NO_2}$(CPFM)) are available for nearly all POLARIS flights at the 15% uncertainty level [*McElroy et al.*, 1995].

The value of $J_{NO_2}$ along the ER-2 flight track was also calculated from standard radiation models using a variety of environmental inputs and assumptions. Three such calculations of $J_{NO_2}$ are compared in this analysis. All three were calculated with isotropic, spherical, multiple-scattering models of the atmospheric radiation field and incorporate temperature-dependent photolysis cross sections for $NO_2$. The first of these, provided by the Jet Propulsion Laboratory (JPL) and denoted $J_{NO_2}(JPL_{TOMS})$ [*Prather*, 1981], uses values of UV reflectivity (a surrogate for albedo) from version 7 Earth Probe Total Ozone Mapping Spectrometer (EP-TOMS) and climatological cloud heights from the International Satellite Cloud Climatology Project (ISCCP) to calculate specific J values along the flight track. The partial ozone column above the ER-2 for the present study is most often estimated from CPFM data, and the total ozone column is constrained to match observations from TOMS. The other two calculations are provided by the Johns Hopkins University Applied Physics Laboratory (APL) [*Anderson et al.*, 1995]. Both APL calculations use standard background aerosol climatologies described in the Air Force Geophysics Laboratory (now Phillips Laboratory) Handbook of Geophysics. Composite ozone profiles, one for each of the three deployments, were obtained from balloon ozonesondes launched from Fairbanks, Alaska, during the POLARIS campaign. The first of these calculations, denoted $J_{NO_2}(APL_{TOMS})$, uses TOMS inputs for surface UV reflectivity as in the JPL calculation. The second, denoted $J_{NO_2}(APL_{CPFM})$, uses albedo and overhead $O_3$ as measured by the CPFM as inputs to the calculation. For both model calculations, if the input albedo

was intermediate between that for terrain (0.08) and that for cloud (0.8), $J_{NO_2}$ was calculated as the linear combination of both the terrain-only (cloud-free) and cloud-only cases. The observed albedo was used to determine the fractional cloud cover. Because the horizontal resolution of CPFM measurements from the ER-2 is much better than that of the TOMS data, $J_{NO_2}$(CPFM) and $J_{NO_2}(APL_{CPFM})$ may exhibit differences due to local changes in cloud cover along the flight track that are not resolved by the TOMS satellite data. The uncertainty associated with calculated values of $J_{NO_2}$ is expected to be ~20% primarily due to uncertainties in the absorption cross section of $NO_2$ [*DeMore et al.*, 1997].

The values of $J_{NO_2}$ found by the various models are highly correlated despite minor differences in the approaches. A comparison of $J_{NO_2}$ values for a single flight is given in Plate 1. As shown in the plate, there are differences between the various estimates of $J_{NO_2}$. The comparisons of $J_{NO_2}$ found by the various radiation field models demonstrate the uncertainty due to different assumptions concerning albedo, as well as possible differences between the models that seek to solve the same set of radiative transfer equations. The systematic difference between the CPFM estimate of $J_{NO_2}$ and that found from all of the radiation field models may indicate a problem either in the calculation or measurement of actinic flux. These differences lie within our estimate of 20% uncertainty for $J_{NO_2}$ used here. In addition, the $J_{NO_2}$(CPFM) and $J_{NO_2}(APL_{CPFM})$ results give values consistently lower than the other calculations. These differences are most likely related to parameters such as albedo or cloud height, which may have a significant effect on $J_{NO_2}$, rather than overhead $O_3$, which has very little impact. The comparison to $J_{NO_2,ss}$ will be discussed in more detail in a later section. However, it should be noted that the average difference between $J_{NO_2,ss}$ and values of $J_{NO_2}$ for flight #II-5 is among the largest seen during POLARIS. The average discrepancy for a given deployment or for the mission as a whole is lower, as shown later.

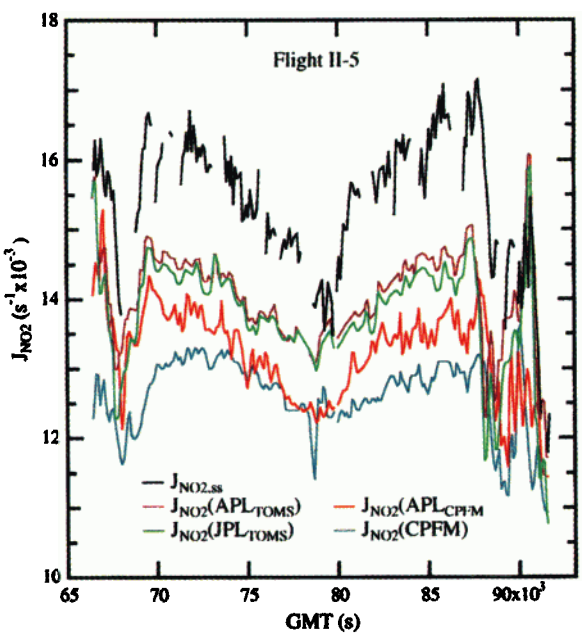


**Plate 1.** Values of $J_{NO_2}$ versus Greenwich Mean Time (s) for Flight #II-5 (see Table 1) as derived from several sources. $J_{NO_2,ss}$ is calculated using the steady state relationship in equation (2) and $[NO_2]_{AL}$ observations. Values of $J_{NO_2}$(CPFM), $J_{NO_2}(APL_{CPFM})$, $J_{NO_2}(APL_{TOMS})$, and $J_{NO_2}(JPL_{TOMS})$ are interpolated to 100-second intervals; $J_{NO_2,ss}$ is calculated from 10-second data and averaged to 100-second intervals. The average difference between $J_{NO_2,ss}$ and each of the values of $J_{NO_2}$ for this flight is among the largest of all POLARIS flights (~ 7 to 18%).

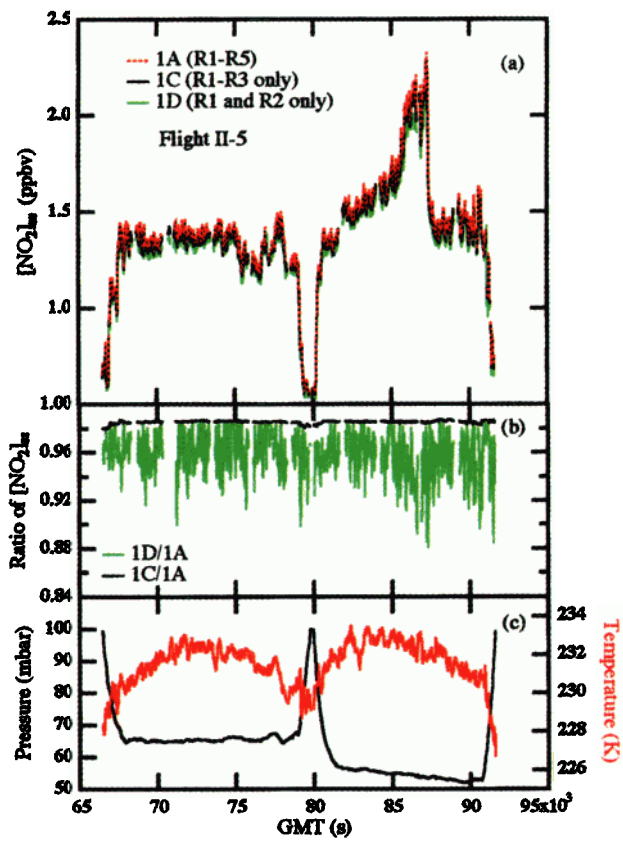


**Plate 2.** Calculations and observations for flight #II-5 versus GMT (see Table 1). (a) Comparison of $[NO_2]_{ss}$ values as calculated from equation (1a) (red, dotted), (1c) (black), and (1d) (green). Results for (1b) are not shown because differences from (1a) are too small to discern. All calculations use $J_{NO_2}(APL_{CPFM})$ as the $NO_2$ photolysis rate coefficient. (b) Ratio of results in Plate 2a: (1d/1a) (green); (1c/1a) (black). (c) Corresponding temperatures (red) and pressures (black) along the flight track. Values of $[NO_2]_{ss}$ and their ratios are calculated from 10-s data. Pressure and temperature are averaged to 10-s intervals.

### 2.4. $[NO_2]_{ss}$ Calculations

In some previous evaluations of the $NO/NO_2$ steady state, $[NO_2]_{ss}$ was calculated using only (R1), (R2), and (R3) (equation (1c)) [*Jaeglé et al.*, 1994]. This treatment is expected to be valid based on the relative values of the (R4) and (R5) terms, which are significantly less than those of (R1)–(R3) [*DeMore et al.*, 1997]. The relative contributions of the associated terms to the value of $[NO_2]_{ss}$ for the Arctic spring, early summer, and late summer seasons have been evaluated using measured $O_3$, ClO, and $HO_2$, and modeled BrO. For these calculations, 1-s $[NO_2]_{AL}$, $O_3$, pressure, and temperature observations were averaged over 10 s. Values of $J_{NO_2}$ (typically reported every 50 to 150 s), ClO (reported every 35 s), and modeled BrO (reported every 100 s) were interpolated to every 10 s. Values of $HO_2$ were interpolated to 1-s data and averaged over 10 s to remove gaps in the reported data. Increased scatter in $[NO_2]_{ss}$ may be expected from the interpolation because of local variations along the flight track that are not resolved.

The results for three calculations of $[NO_2]_{ss}$ made for flight #II-5 are shown in Plate 2a. Ratios of the calculated values are shown in Plate 2b. Because (R3)-(R5) all represent NO loss processes and $J_{NO_2}$ is the same in each calculation, relative differences in the value of $[NO_2]_{ss}$ for each calculation are equivalent to relative differences in the total loss of NO. From these ratios it is shown that the combined contribution of the $HO_2$ and BrO terms to the total NO loss is less than 2.5% over the entire flight track. In contrast, the combined contribution of the ClO, $HO_2$, and BrO terms ranges from 4 to 8%. The average results for each season are shown in Table 4.

The contribution of the $HO_2$ and BrO terms has been evaluated previously as part of the error analysis by *Jaeglé et al.* [1994] to be <1% and approximately 2%, respectively, at Northern Hemisphere midlatitudes, consistent with the results shown in Table 4. BrO values in the *Jaeglé et al.* [1994] study were estimated from a climatology developed by *Wennberg et al.* [1994] based on in situ observations. In evaluations of $[NO_2]_{ss}$ for the Southern Hemisphere (45°S - 68°S), *Gao et al.* [1997] found an average BrO contribution of approximately 3%. In the *Gao et al.* [1997] study, BrO values were estimated from compact relationships between BrO and CFC-11 and between CFC-11 and $N_2O$ [*Woodbridge et al.*, 1995]. Each of these studies, including the results presented here, indicates that BrO and $HO_2$ do not make a large contribution to the value of $[NO_2]_{ss}$. The contributions of each of these terms may become more significant under specific conditions. For example, during the polar winter when mixing ratios of ClO are significantly elevated due to heterogeneous processing, the contribution of this term to the expression will become more competitive with the $O_3$ term. Similarly, at altitudes closer to the tropopause where the relative mixing ratios of inorganic chlorine species decrease substantially, the contribution of the $HO_2$ term to the expression may become competitive with that of ClO. Therefore, despite the small contribution from these terms, $[NO_2]_{ss}$ is calculated using all terms (equation (1a)) in the remaining analysis for completeness.

**Table 4.** Fractional Contributions to $[NO_2]_{ss}$ From Terms in Equation (1a).

| Term | POLARIS Deployment[a] | | |
|---|---|---|---|
| | April/May | June/July | September |
| (R3) ClO | 5.0 | 3.4 | 6.1 |
| (R4) BrO | 1.7 | 1.5 | 2.5 |
| (R5) $HO_2$[b] | 0.4 | 0.4 | 0.5 |
| (R3)-(R5) all | 7.1 | 5.3 | 9.1 |

Contributions are in percent.

[a] Flights listed in Table 1.

[b] Seasonal differences in the contribution of the $HO_2$ term are not statistically significant.

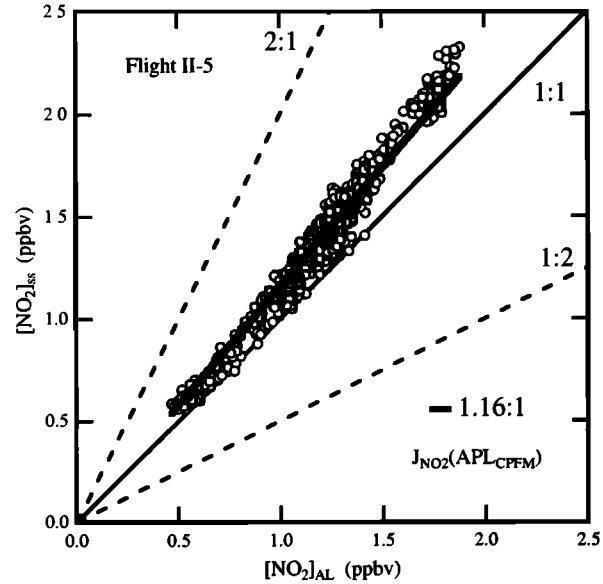


**Figure 5.** Comparison of $[NO_2]_{ss}$ (equation (1a)) with $[NO_2]_{AL}$ for flight #II-5 (see Table 1). The best linear fit through the 10-second $[NO_2]_{ss}$ data (when forced through the origin) has a slope of 1.16 (thick solid line). The average difference between $[NO_2]_{ss}$ and $[NO_2]_{AL}$ for this flight is among the largest for all POLARIS flights.

## 3. Results and Discussion

### 3.1. $[NO_2]_{ss}$ Evaluation

A comparison of $[NO_2]_{ss}$ with $[NO_2]_{AL}$ for flight #II-5 is shown in Figure 5. The slope of the unweighted linear fit through all points for that flight indicates that $[NO_2]_{ss}$ is 16% higher than $[NO_2]_{AL}$ on average. As found in the previous studies noted above, the average difference between $[NO_2]_{ss}$ and measured $NO_2$ is within the combined instrumental and model uncertainties (as discussed below). In addition, as noted above for Plate 1, discrepancies for this flight are among the largest of all POLARIS flights.

The comparison in Figure 5 shows the discrepancy for a single flight when $[NO_2]_{ss}$ is calculated using

$J_{NO_2}(APL_{CPFM})$. The average results for all of POLARIS are shown separately in Plate 3 for all four sets of $J_{NO_2}$ values. The validity of equations (1a)-(1d) is generally limited to solar zenith angles (SZAs) <85°. At higher SZAs the magnitude of $J_{NO_2}$ is considerably smaller than at low SZAs, and the rate of change of $J_{NO_2}$ is considerably larger. The combination of these changes for POLARIS sampling conditions results in an imbalance in $NO_2$ production and loss rates, making the steady state assumption invalid in many cases. As a result, the data set shown in Plate 3 only includes data taken when SZA ≤85°. The slopes of the linear fits to the data shown in Plate 3 indicate that average differences between $[NO_2]_{SS}$ and $[NO_2]_{AL}$ for the whole campaign range from 4 to 19% for all J values used. $J_{NO_2}(JPL_{TOMS})$ values are consistent with $J_{NO_2}$ values used by *Gao et al.* [1997], although improvements in the radiation field model and its inputs makes them slightly different. The results of the $[NO_2]_{SS}$ comparison in the *Gao et al.* [1997] study and the results of the comparison using $J_{NO_2}(JPL_{TOMS})$ in the present study are also consistent. In the present study, values of $[NO_2]_{SS}$ exceed $[NO_2]_{AL}$ by 7% on average when $J_{NO_2}(JPL_{TOMS})$ is used, while the *Gao et al.*, [1997] study found differences of approximately 8%. However, if a different value of $J_{NO_2}$ is used in the calculation, the discrepancies between $[NO_2]_{SS}$ and $[NO_2]_{AL}$ appear either larger ($J_{NO_2}(CPFM)$ and $J_{NO_2}(APL_{CPFM})$) or smaller ($J_{NO_2}(APL_{TOMS})$). Because albedo and cloud height are expected to have a stronger influence on values of $J_{NO_2}$ than overhead ozone, values of $J_{NO_2}(APL_{CPFM})$ and $J_{NO_2}(CPFM)$ (Plate 3a and 3c) are expected to show strong similarities, as are $J_{NO_2}(JPL_{TOMS})$ and $J_{NO_2}(APL_{TOMS})$ (Plate 3b and 3d). In all cases, the range of agreement with different J values falls within the expected 20% uncertainty in calculated $J_{NO_2}$. Average differences are smaller when comparisons are made using $[NO_2]_{HU}$ data. In such comparisons, linear fits to the available data set (see Table 1) show discrepancies ranging from -5 to 6%. In addition, both $NO_2$ data sets show similar nonlinearities and seasonal differences in comparisons with $[NO_2]_{SS}$, as discussed later.

The color scale shown in Plate 3 indicates the average fractional solar exposure for the last 5 days of an air parcel's history. The solar exposure parameter is calculated using each air parcel's 5-day back trajectory (Goddard Space Flight Center trajectory model output) and integrating the fraction of time spent at SZA <93°. Thus an air parcel at the equator experiencing a typical diurnal cycle of illumination would have an average solar exposure of 0.5, while air parcels experiencing continuous sunlight will have a solar exposure of 1.0. As noted above in the discussion related to Figure 1, continuous solar illumination is expected to enhance mixing ratios of $NO_2$ relative to total $NO_y$. The average $NO_y$ value at cruise altitudes is similar for all three POLARIS deployments (Table 1). The comparisons in Plate 3 show that the highest values of $NO_2$ occur in air parcels that experience continuous sunlight, in agreement with expectations. Although solar exposure is not expected to affect the $NO_2$/NO steady state, this parameter is used to highlight the data corresponding to these unique photochemical conditions.

The black points in Plate 3 represent averages of 2000 data points, each of which represents 10 s of in situ data. The vertical and horizontal bars correspond to the 1-σ standard deviation of $[NO_2]_{SS}$ and $[NO_2]_{AL}$ values, respectively, contained in the average. From these averaged data, the curvature in the relationship between $[NO_2]_{SS}$ and $[NO_2]_{AL}$ becomes apparent. At low values of $[NO_2]_{AL}$ (0.0 to 0.5 ppbv), $[NO_2]_{SS}$ values are greater than $[NO_2]_{AL}$ by 5 to 14% using $J_{NO_2}(CPFM)$ (Plate 3c). At higher values of $[NO_2]_{AL}$ (1.0 to 1.5 ppbv), $[NO_2]_{SS}$ exceeds $[NO_2]_{AL}$ by as much as 18 to 24% for this comparison. Similarly, average discrepancies range from -7 to 3% at values of 0.0 to 0.5 ppbv using $J_{NO_2}(APL_{TOMS})$, $J_{NO_2}(APL_{CPFM})$, and $J_{NO_2}(JPL_{TOMS})$ (Plate 3a, 3b, and 3d) but range from 5 to 12% at values of 1.0 to 1.5 ppbv. These results are consistent with the study of *Gao et al.* [1997] in which mixing ratios of $NO_2$ were typically less than 0.5 ppbv. A similar curvature exists when comparisons are made of $[NO_2]_{SS}$ with $[NO_2]_{HU}$ (-7% at low values, -2% at high values). Moreover, the relationship between $[NO_2]_{AL}$ and $[NO_2]_{HU}$ appears to be linear over this range, indicating that a systematic $NO_2$ measurement error is an unlikely source of this nonlinearity.

Despite the coincidence of points with large discrepancies and high solar exposures, solar exposure cannot conclusively be linked to any systematic impact on discrepancies between $[NO_2]_{SS}$ values and measured values. Points corresponding to a solar exposure of 1.0 arise predominantly from flights during Deployment II of POLARIS, although some flights during Deployments I and III reached solar exposures of 1.0. However, even high solar exposure data from Deployments I and III have smaller average discrepancies than similar data from Deployment II. Thus while there are seasonal differences in the magnitude of the discrepancy between $[NO_2]_{SS}$ and $[NO_2]_{AL}$, these differences do not appear to be directly related to solar exposure. Similar seasonal differences are noted in comparisons using $[NO_2]_{HU}$.

### 3.2. $J_{NO_2,SS}$

The steady state expression shown in equation (2) for calculation of $J_{NO_2,SS}$ was also evaluated. The results for flight #II-5 using $[NO_2]_{AL}$ are shown in Plate 1. $J_{NO_2,SS}$ is greater than the other calculated values of $J_{NO_2}$ by 7 to 18%, depending on the specific J value used in the comparison. This result is consistent with the fact that values of $[NO_2]_{SS}$ are higher than measured values by 8 to 19% for this flight (Figure 5).

The combined results for $J_{NO_2,SS}$ are shown in Plate 4. As in Plate 3, the linear fit for each comparison is shown by the red line, and data are selected for SZA <85°, for which the steady state expression is expected to be valid. The colored points represent average values for individual flights with horizontal and vertical bars representing the 1-σ standard deviation of $J_{NO_2}$ and $J_{NO_2,SS}$ values, respectively, for that

flight. Mean discrepancies (from the slope of the linear fits) between $J_{NO_2,ss}$ and derived values of $J_{NO_2}$ are smaller than discrepancies seen in comparisons of $[NO_2]_{ss}$ and $[NO_2]_{AL}$. However, the range of discrepancies is magnified in Plate 4 by the smaller dynamic range of $J_{NO_2}$ compared to $[NO_2]$. Owing to this magnification, the magnitude of the discrepancy varies more between flights than within a given flight. By comparing deployments in Plate 4 (colored points), seasonal differences are apparent in the comparisons of $J_{NO_2,ss}$ as in the comparisons of $[NO_2]_{ss}$. In the $J_{NO_2}(APL_{TOMS})$ case (Plate 4b), for which the linear fit indicates minimal differences with $J_{NO_2,ss}$ (~1%), the six flights from Deployment II have average differences of +8%, balancing average differences of -3% for flights during Deployments I and III. The summer period during POLARIS is characterized by relatively higher solar exposure, lower solar zenith angles, and higher levels of NO and $NO_2$ in comparison to the other seasons sampled. In addition, due to the extended illumination, temperature is also elevated somewhat during the summer period, leading to an increased rate for (R2). The combination of all of these parameters in affecting calculations of $J_{NO_2}$ precludes a simple identification of the source or sources of the seasonal differences. Further analysis of the seasonal differences is provided in a later section.

### 3.3. Estimated Uncertainties

Uncertainties for the individual measurements used in the calculation of $[NO_2]_{ss}$ and $J_{NO_2,ss}$ are given in Table 2. BrO values from the PSS model depend, in part, on whether the model is constrained by values of NO or $NO_y$ because of the well-documented difficulties in simulating the observed $NO/NO_y$ ratio [*Gao et al.*, 1999; *Osterman et al.*, 1999]. The NO-constrained model gives BrO values that are consistently ~17% greater than the $NO_y$-constrained BrO values for all POLARIS flights. As noted previously, for this analysis an NO-constrained model run was used for BrO. A previous study by *Avallone et al.* [1995] indicated that photochemical model calculations tend to overestimate the BrO fraction of $Br_y$ by as much as 25%. The uncertainty associated with BrO in this study is estimated to be ±25%.

Systematic errors in the values of BrO and $HO_2$ have relatively little influence on the value of $[NO_2]_{ss}$ and cannot account for the discrepancies of 4 to 19% found between $[NO_2]_{ss}$ and $[NO_2]_{AL}$. The BrO and $HO_2$ terms in equation (1a) are at least an order of magnitude smaller than the other terms in the expression. Thus even 15 to 20% changes to these mixing ratios will have less than a 1% effect on calculated values of $[NO_2]_{ss}$. Similarly, the 15% uncertainty associated with the ClO mixing ratio has little impact on the comparison. The ClO term becomes most competitive with the $O_3$ term at the lowest temperatures, making a maximum contribution to the uncertainty of 4% at 195 K and <1% at 235 K. Systematic errors in the mixing ratios of NO and $O_3$ potentially could make a 4 to 6% difference in the comparison, but cannot account for discrepancies of 19%. Values of $NO_2$ and $J_{NO_2}$ have a more direct influence on the agreement between $[NO_2]_{ss}$ and $[NO_2]_{AL}$, and the uncertainties associated with these values are sufficient to account for the average discrepancies found in each comparison.

In addition to the uncertainties associated with radical mixing ratios, there are significant uncertainties associated with the rate coefficients for (R2)–(R5). For the temperatures encountered during POLARIS (195 to 235 K) the uncertainty for these rate coefficients ranges from 59 to 80% [*DeMore et al.*, 1997], much larger than that estimated for any of the radical measurements, values of $J_{NO_2}$, or modeled BrO. As a result, the rate coefficient uncertainty is the dominant contribution to the uncertainty in each term in the numerator of equations (1a) and (2). The largest contribution to the total uncertainty in the calculation of $[NO_2]_{ss}$ and $J_{NO_2,ss}$ is that associated with (R2) ($k_2[O_3]$). The recommended uncertainty in the value of $k_2$ is ±59 to 70% at POLARIS temperatures [*DeMore et al.*, 1997]. Because the value of the (R2) term is generally an order of magnitude larger than the (R3)-(R5) terms, this uncertainty outweighs all others.

The previous study by *Jaeglé et al.* [1994] suggested that reducing the recommended rate coefficient for (R2) by 35% (or by 25% with a 15% increase in $J_{NO_2}$) would allow steady state and measured concentrations of $NO_2$ to be reconciled. *Gao et al.* [1997] found agreement between $[NO_2]_{ss}$ and $[NO_2]_{AL}$ to be within 8% and determined that large changes to rate coefficients and photolysis rates were unnecessary. The comparisons presented here are in agreement with the *Gao et al.* [1997] study. *Sen et al.* [1998] examined the laboratory observations used in the *DeMore et al.* [1997] evaluation of this rate and concluded that it was difficult to rule out the possibility that the actual rate of (R2) is 15% faster than the *DeMore et al.* [1997] rate for temperatures near 216 K. This faster rate would lead to better agreement between models and the MkIV measurements of NO and $NO_2$ but would worsen the agreement found here. Any change to $k_2$ or $J_{NO_2}$ that effectively corrects the comparison for POLARIS data from Deployments I and III will not remove the discrepancy noted for Deployment II (see next section).

The recommended value of $k_2$ is based on the results of five independent laboratory studies with stated uncertainties of ±10 to 20% [*DeMore et al.*, 1997, and references therein; see also *Sen et al.*, 1998, Figure 7]. At 298 K, the range of the five values of $k_2$ falls within these uncertainties. However, at the lower temperatures encountered during POLARIS the range in laboratory determinations of $k_2$ increases to ±22 to 40% relative to the recommended value. Although these uncertainties are accounted for in the *DeMore et al.* [1997] estimate of the uncertainty of $k_2$, using $k_2$ from one of the five studies in place of the recommended rate coefficient results in significant differences in the calculated value of $[NO_2]_{ss}$ or $J_{NO_2,ss}$. For example, using the fit recommended by *Borders and Birks* [1982] in which curvature in the temperature dependence of $k_2$ was measured results in average discrepancies of +21% between $[NO_2]_{ss}$ and $[NO_2]_{AL}$. A new expression for $k_2$ was recently

measured at tropospheric temperatures and pressures by *Moonen et al.* [1998] in response to discrepancies in the partitioning of NO and $NO_2$ found in tropospheric field studies. Using this new expression for $k_2$ yields average discrepancies between $[NO_2]_{ss}$ and $[NO_2]_{AL}$ of -17% due to a higher value for the Arrhenius parameter and a smaller positive temperature dependence. Both the *Borders and Birks* [1982] and the *Moonen et al.* [1998] studies included measurements down to 200 to 205 K, and the values of $k_2$ calculated using these expressions represent the high and low extremes, respectively, for temperatures encountered during POLARIS. Significant improvements can be made in our evaluation of the steady state relationship between NO and $NO_2$ if the uncertainty of the rate coefficient of (R2) can be reduced.

When the uncertainties in the rate coefficients for (R2)-(R5) and the values of the radical species and $J_{NO_2}$ are combined, the ± 1-σ uncertainty in $[NO_2]_{ss}$ ranges from ±49 to 64% for the pressure and temperature conditions encountered during POLARIS. $J_{NO_2,ss}$ has a similar uncertainty, ranging from ±54 to 68%. These error estimates do not include a small reduction in uncertainty expected due to the common calibration standard used for the NO and $NO_2$ channels of the NOAA instrument (~1 to 3%). The agreement shown in all comparisons in this analysis falls well within these estimated uncertainty ranges.

### 3.4. Seasonal Differences in $[NO_2]_{ss}$ and $J_{NO_2,ss}$

Despite the general agreement between $[NO_2]_{ss}$ and measured $NO_2$ (and between $J_{NO_2,ss}$ and measured or modeled $J_{NO_2}$), the source of the seasonal differences noted in the discussions of Plates 3 and 4 remains unidentified. No changes in instrument sensitivity, background signal, or absolute calibration have been found that can explain a systematic difference of ~10% in the measurements of NO, $[NO_2]_{AL}$, or $[NO_2]_{HU}$ between deployments. As noted above, because similar systematic behavior appears in two independent measurements of $NO_2$, measurement error in $NO_2$ seems an unlikely explanation. Interference due to thermal decomposition of other $NO_y$ species, which could potentially be a factor in both $NO_2$ measurements, would cause $NO_2$ values to be overestimated. This interference would be most apparent in the early summer deployment due to elevated ambient temperatures, yet the comparison with $[NO_2]_{ss}$ indicates the opposite behavior. The similarity of the seasonal dependence of the discrepancy for all four values of $J_{NO_2}$ cannot be used to rule out the possibility that uncertainty in $J_{NO_2}$ is the cause of the seasonal differences. However, any source of the seasonal differences must arise from a parameter common to all four calculations, such as the temperature dependence of the $NO_2$ cross section or problems with the measurement of albedo at low values. Other physical reasons for the difference between deployments are difficult to distinguish. Since the rates of (R1) and (R2) have the largest effect on the value of $[NO_2]_{ss}$, the effect of season on these rates was evaluated in detail. Plate 5 shows the ratio $[NO_2]_{ss}/[NO_2]_{AL}$ as a function of temperature. In this plate, the discrepancies between $[NO_2]_{ss}$ and $[NO_2]_{AL}$ are shown by deviations of $[NO_2]_{ss}/[NO_2]_{AL}$ from unity (black line). As shown in Plate 5a, the largest positive discrepancies are associated with the highest temperatures. This apparent dependence on temperature also correlates well with the rate of (R2) as shown in the color scale. Because (R2) has a positive temperature dependence, the highest temperatures correspond to the fastest production of $NO_2$, in the same direction as the discrepancy. A linear fit to the data in Plate 5a gives a slope of 0.007 ($r^2$ = 0.5; $r^2$ is the linear correlation coefficient for which values of 1 indicate complete correlation, while values near zero indicate no correlation), corresponding to a 7% increase in the discrepancy for every 10 K increase in temperature. As shown in Plate 5b, the largest positive discrepancies are also associated primarily with Deployment II, making it difficult to define a single temperature dependence for the entire data set. Linear fits to the data for individual deployments give slopes that range from 0.002 to 0.012 ($r^2$ < 0.4 in all cases), with Deployment II showing the strongest dependence. Thus, the small apparent temperature dependence is not statistically significant.

A similar comparison is shown in Plate 6, with $[NO_2]_{ss}/[NO_2]_{AL}$ plotted as a function of SZA. The apparent curvature in this relationship at SZA > 60° (Plate 6a) is removed when the data are separated by deployment. Points corresponding to Deployment II appear to be offset from the remaining data (Plate 6a). However, there is no overall dependence of the ratio on SZA. In addition, using the color scale for Plate 6a, no significant correlation with $J_{NO_2}$ is apparent in this relationship. Similar comparisons were made for a variety of other parameters. No direct dependence could be discerned for albedo, overhead $O_3$, pressure, or potential temperature; or for mixing ratios of $O_3$, $NO_y$, ClO, BrO, and $HO_2$. Although there may be a small dependence on temperature or the rate of (R2), the magnitude of the dependence is not statistically significant or uniform for all deployments, and therefore a cause of the seasonal differences in the $[NO_2]_{ss}$ comparison cannot be identified here.

The contribution to equation (1a) of other reactions not considered here remains a possibility to explain the seasonal differences. Recent studies have addressed the possibility that heterogeneous reactions of $NO_2$ on aerosol surfaces may play a role in the stratosphere [*Gao et al.*, 1998; *Langenberg et al.*, 1998; *Lary et al.*, 1997; *Kleffman et al.*, 1998; *Rogaski et al.*, 1997; *Tabor et al.*, 1994]. These studies have focused primarily on the direct production of NO through reaction of $NO_2$ on soot surfaces and the reaction of $NO_2$ on sulfate surfaces to produce HONO, which photolyzes to produce NO. *Lary et al.* [1997] proposed that reactions of $NO_2$ on soot surfaces could be an additional mechanism for production of NO and, indirectly, loss of $O_3$. *Gao et al.* [1998] have used in situ observations in a Concorde aircraft plume to derive an upper limit for this reaction rate. Using a reactive uptake coefficient ($\gamma_{NO_2}$) of

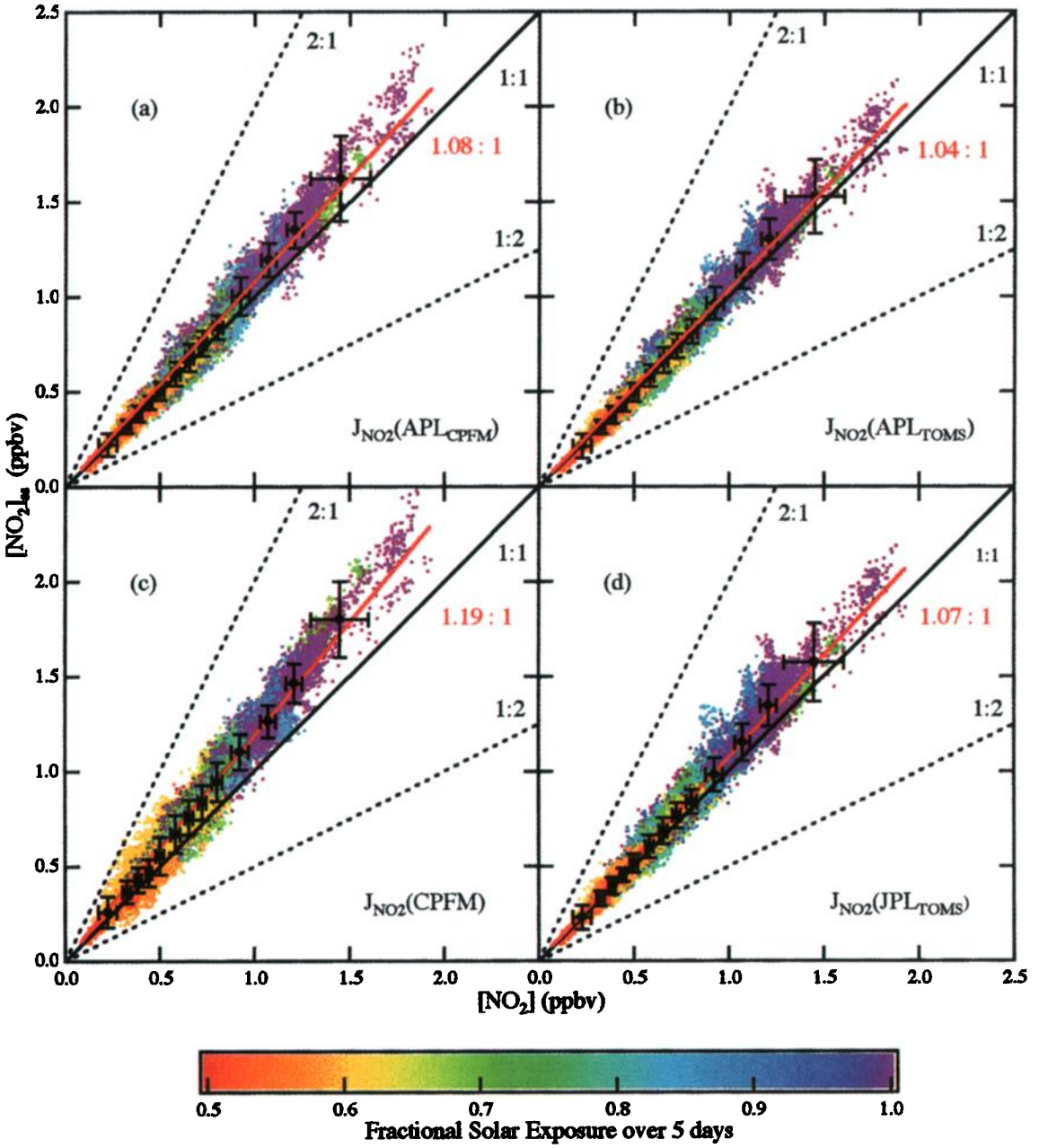


**Plate 3.** Cross plot of $[NO_2]_{ss}$ calculated using equation (1a) and $[NO_2]_{AL}$ for all available POLARIS flights (see Table 1). Values of $[NO_2]_{ss}$ are calculated using $J_{NO_2}$ from (a) $J_{NO_2}(APL_{CPFM})$, (b) $J_{NO_2}(APL_{TOMS})$, (c) $J_{NO_2}(CPFM)$, and (d) $J_{NO_2}(JPL_{TOMS})$. Each panel contains approximately 30,000 data points. Data are reported every 10 s and selected for SZA < 85° and (50 mbar < pressure < 100 mbar). Red lines represent the best linear fit through the data for each comparison when constrained to pass through the origin. ($J_{NO_2}(CPFM)$ data have been filtered to remove extreme outliers.) Black lines represent the 1:1 correlation line (solid) and the 1:2 and 2:1 correlation lines (dashed). The color of individual points represents the associated average fractional solar exposure of the air mass over 5 days prior to sampling, as designated in the color scale. Black points represent 2000-point averages of both $[NO_2]_{ss}$ and $[NO_2]_{AL}$ values. Vertical and horizontal bars on these points represent the 1-σ standard deviation of data contained in the average.

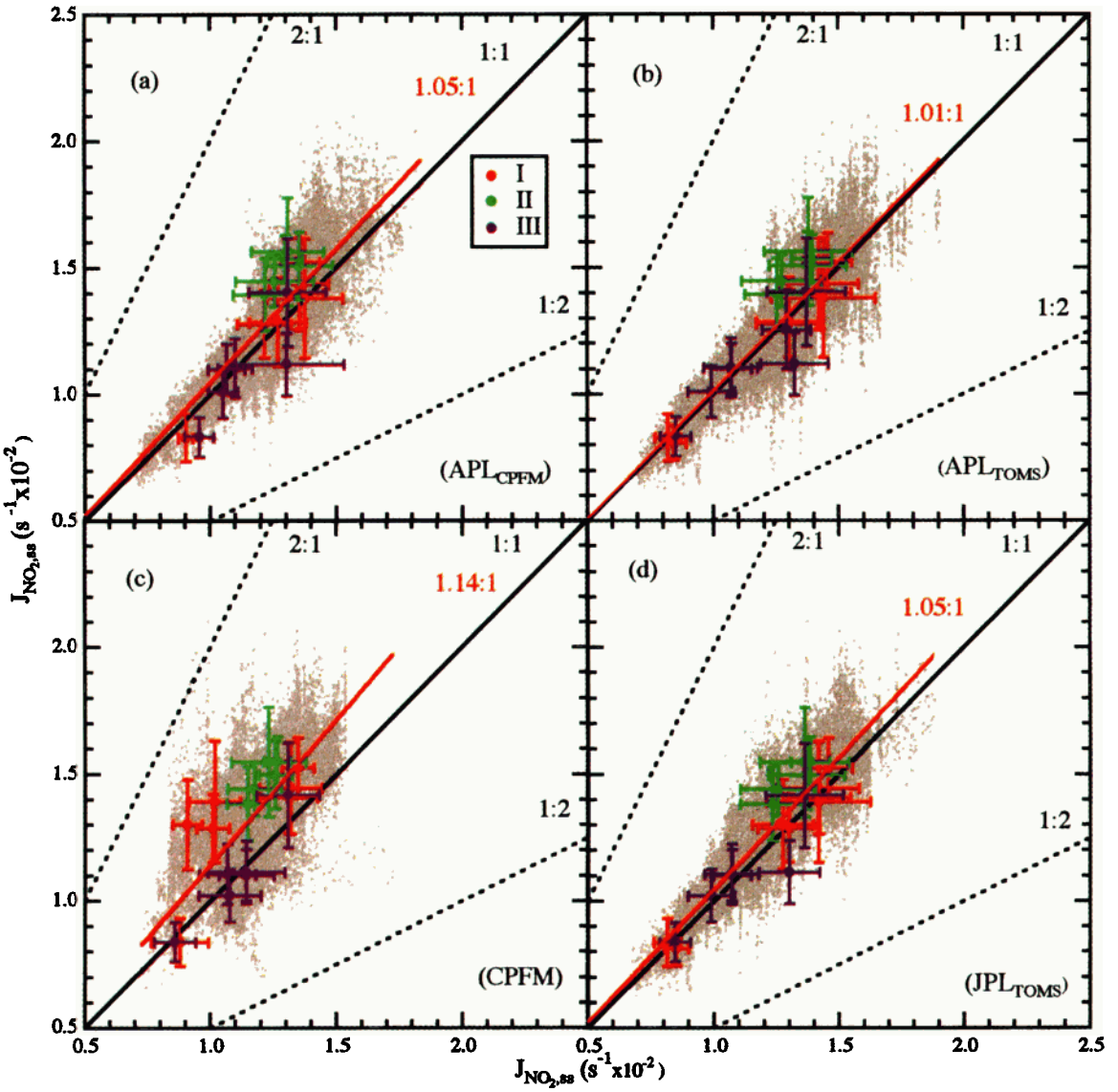


**Plate 4.** Cross plot of $J_{NO_2,ss}$ calculated using equation (2) for all available POLARIS flights and $J_{NO_2}$ from (a) $J_{NO_2}(APL_{CPFM})$, (b) $J_{NO_2}(APL_{TOMS})$, (c) $J_{NO_2}(CPFM)$, and (d) $J_{NO_2}(JPL_{TOMS})$. Each panel contains approximately 30,000 data points. Data are 10-s averages selected for SZA < 85° and (50 mbar < pressure < 100 mbar). Red lines represent the best linear fit through the data for each comparison when constrained to pass through the origin. ($J_{NO_2}$(CPFM) data have been filtered to remove extreme outliers.) The colored points represent average values for individual flights and vertical and horizontal bars represent the 1-σ standard deviation of $J_{NO_2,ss}$ and $J_{NO_2}$ values, respectively, that are included in the average. The colors represent deployment I (spring, red), deployment II (early summer, green), and deployment III (late summer, purple).

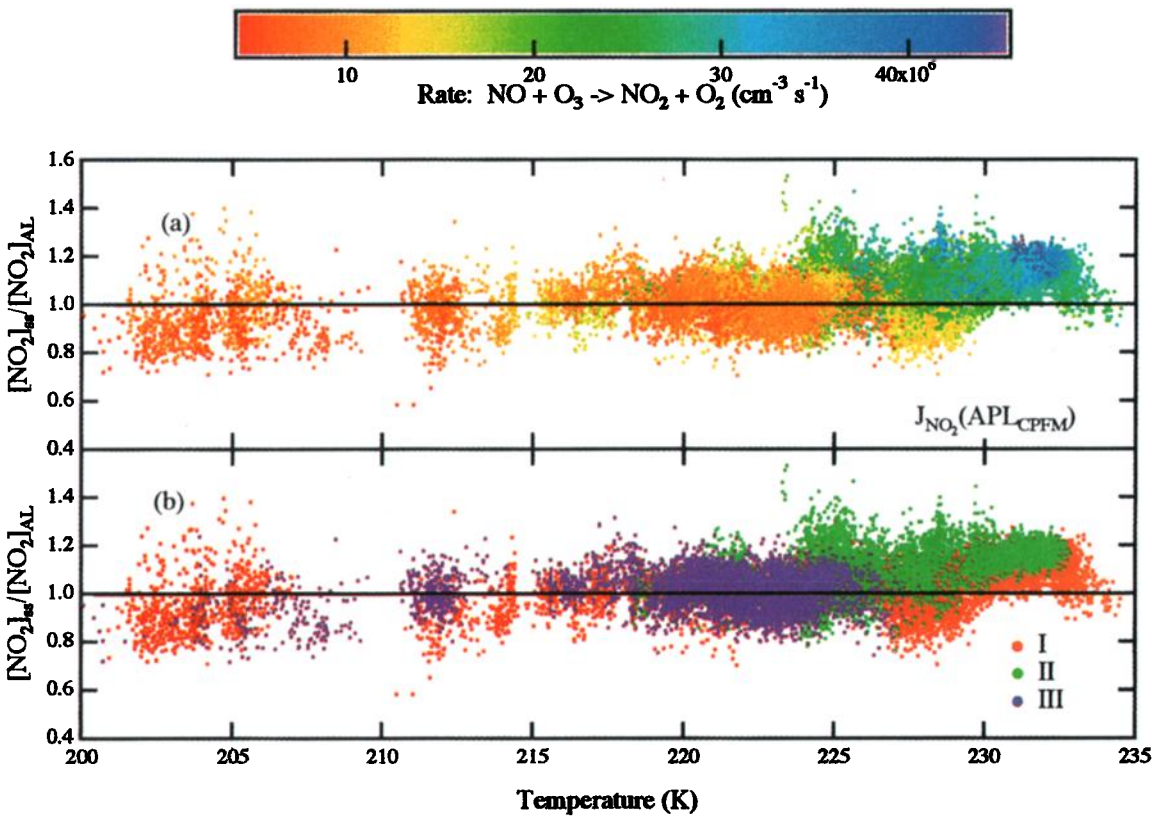


**Plate 5.** Ratio of $[NO_2]_{SS}$ and $[NO_2]_{AL}$ values plotted as a function of temperature. Data are 10-s averages selected for SZA < 85° and (50 mbar < pressure < 100 mbar). (a) Colored points show the associated rate of reaction (R2) using the color scale at the top. (b) Colors represent the corresponding POLARIS deployment (Table 1).

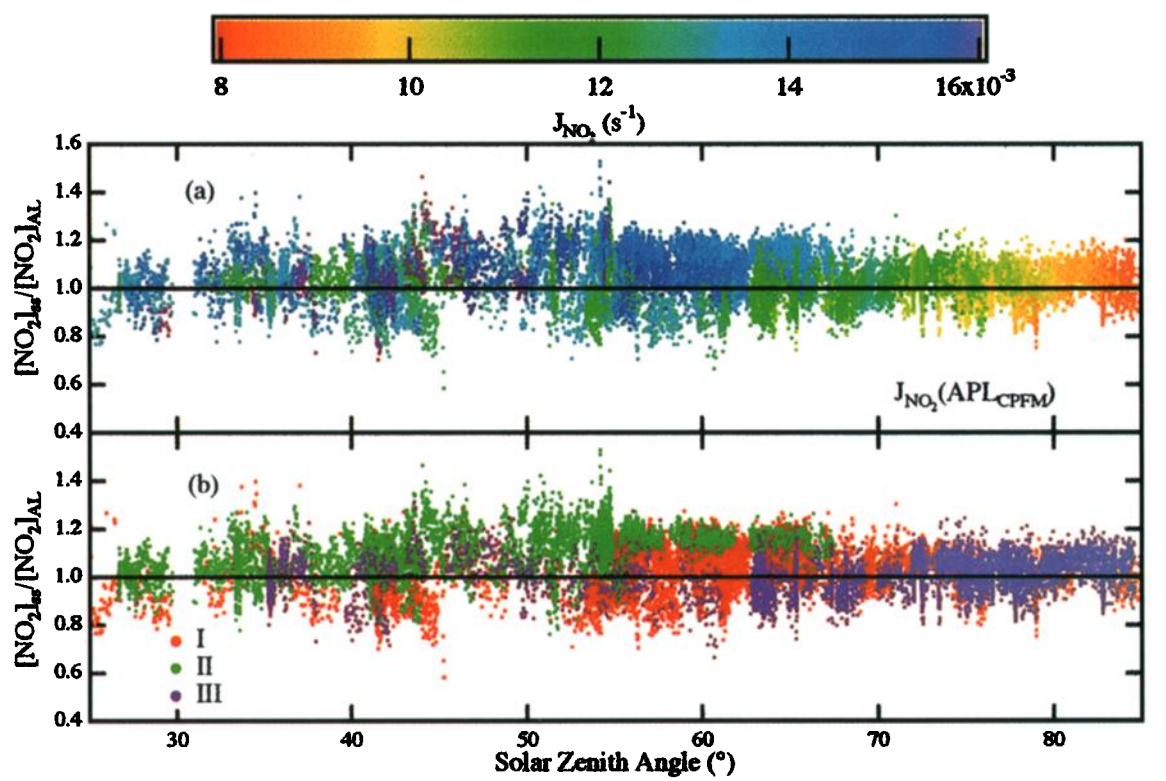


**Plate 6.** Ratio of $[NO_2]_{SS}$ and $[NO_2]_{AL}$ values plotted as a function of SZA. Data are 10-s averages selected for SZA < 85° and (50 mbar < pressure < 100 mbar). (a) Colored points show the value of $J_{NO_2}$ as shown in the color scale at the top. (b) Colors represent the corresponding POLARIS deployment (Table 1).

$1.7 \times 10^{-5}$, derived by *Gao et al.* [1998] and soot surface area densities derived from *Blake and Kato* [1995] for the background stratosphere, the time constant for this reaction in the lower stratosphere under conditions observed during POLARIS would be of the order of years. The $\gamma_{NO_2}$ value derived by *Gao et al.* [1998] was significantly lower than that used in the modeling study by *Lary et al.* [1997]. However, even using the maximum values proposed by *Lary et al.* [1997], the time constant for this reaction is still greater than 12 hours at stratospheric conditions. Therefore inclusion of this reaction would not alter the steady state values for $NO_2$ found here.

The heterogeneous reaction of $NO_2$ occurring on the surface of sulfate aerosols to produce HONO also does not affect the $NO_2$ steady state expression due to the relatively long time constant for formation of NO via this process. The inclusion of this process in the calculation of $[NO_2]_{ss}$ makes a statistically insignificant (<<1%) difference. Similarly, for background aerosol conditions all heterogeneous reactions of $NO_2$ on sulfate generally can be neglected in the steady state expression. For example, since the POLARIS campaign took place during a volcanically quiescent period in the lower stratosphere, sulfate surface area densities did not exceed 4 $\mu m^2\ cm^{-3}$. The expression for a heterogeneous rate coefficient takes the general form:

$$k_{het} = \gamma_{NO_2} \frac{\langle v \rangle}{4} SA \qquad (4)$$

where $\langle v \rangle$ is the average velocity of an $NO_2$ radical at stratospheric temperatures and pressures, and SA is the sulfate surface area density. Assuming that every collision of $NO_2$ with a sulfate surface leads to reaction and formation of NO ($\gamma_{NO_2} = 1$) and SA = 4 $\mu m^2\ cm^{-3}$, a heterogeneous reaction can only make a 3% change in values of $[NO_2]_{ss}$ when compared with minimum values of $J_{NO_2}$ at SZA < 85° (~ 0.007 $s^{-1}$). When $J_{NO_2}$ is larger, the impact of heterogeneous reactions will be smaller. Therefore such reactions could not account for the seasonal differences or the 4 to 18% average discrepancies in the POLARIS results.

## 4. Conclusions

In situ measurements of NO, $NO_2$, $O_3$, ClO, and $HO_2$ have been obtained in the lower stratosphere (18 to 20 km) over a latitude range of 3°S to 90°N. The bulk of these measurements were made between 60°N and 90°N during the spring, early summer, and late summer seasons as part of the 1997 POLARIS field campaign. Steady state values of $NO_2$ ($[NO_2]_{ss}$) were calculated (equations (1a)-(1d)) using simultaneous observations of NO, $O_3$, $HO_2$, and ClO, gas phase reaction rate coefficient data, and $J_{NO_2}$ (the photolysis rate coefficient of $NO_2$). Values of $J_{NO_2}$ used were either derived from spectroradiometer observations or calculated from radiation field models. Values of $[NO_2]_{ss}$ differ from measured values by up to 25% with average discrepancies between +4 and +8% when values of $J_{NO_2}$ from radiation field models are used in the calculation. Average discrepancies are larger (+19%) when values of $J_{NO_2}$ are obtained from spectroradiometer observations. In all comparisons, the largest discrepancies are found at the highest values of $NO_2$. These differences are considerably smaller than the uncertainties associated with the calculation of $[NO_2]_{ss}$ (~50 to 70%). An additional comparison was made between values of $J_{NO_2}$ as calculated from the in situ measurements ($J_{NO_2,ss}$) and the four values of $J_{NO_2}$ derived from the spectroradiometer and radiation field models. Average discrepancies between $J_{NO_2,ss}$ and $J_{NO_2}$ were smaller than in the $[NO_2]_{ss}$ comparisons (1 to 14%), though the range of the discrepancies was larger. As in the case of $[NO_2]_{ss}$, discrepancies between $J_{NO_2,ss}$ and $J_{NO_2}$ fell within the uncertainty associated with the calculation. A reduction in the uncertainty in the rate coefficient of NO + $O_3$ (R2) would significantly reduce the uncertainty in calculated values of $[NO_2]_{ss}$ and $J_{NO_2,ss}$.

Seasonal differences in the discrepancy between steady state and measured $NO_2$ values were found using the POLARIS data, with larger discrepancies in the early summer season than in spring or late summer. The cause of these differences has not been identified. The consistency between comparisons using two independent measurements of $NO_2$ suggests that $NO_2$ measurement error is an unlikely cause of the seasonal differences.

In comparison with previous studies, the POLARIS results extend the evaluation of $[NO_2]_{ss}$ to a wider range of values of $NO_2$ and $J_{NO_2}$, as well as other species important for the partitioning of NO and $NO_2$. Collectively, the results presented here and in previous studies indicate that average values of $NO_2$ and $[NO_2]_{ss}$ consistently agree within 25% for a broad range of conditions sampled in the sunlit lower stratosphere between the tropics and the pole in both hemispheres.

**Acknowledgments.** The authors gratefully acknowledge T. F. Hanisco and E. J. Lanzendorf for use of the $HO_x$ data set, J. C. Wilson and C. A. Brock for use of the aerosol data set, and P. A. Newman for the calculation of the solar exposure parameter. This work was supported by the NASA Upper Atmosphere Research Program, Atmospheric Chemistry and Modeling and Analysis Program, and the Atmospheric Effects of Stratospheric Aircraft Project of the NASA High Speed Research Program.

## References

Anderson, D. E., R DeMajistre, S. A. Lloyd, and P. K Swaminathan, Impact of aerosols and clouds on the troposphere and stratosphere radiation field with application to twilight photochemistry at 20 km, *J. Geophys. Res., 100*, 7135-7145, 1995.

Avallone, L. M , D. W. Toohey, S. M. Schauffler, W. H. Pollock, L. E. Heidt, E. L. Atlas, and K. R. Chan, In situ measurements of BrO during AASE II, *Geophys. Res. Lett., 22*, 831-834, 1995.

Blake, D. F., and K. Kato, Latitudinal distribution of black carbon soot in the upper troposphere and lower stratosphere, *J. Geophys. Res., 100*, 7195-7202, 1995.

Borders, R. A., and J. W. Birks, High-precision measurements of activation energies over small temperature intervals: Curvature in the Arrhenius plot for the reaction NO + $O_3 \rightarrow NO_2 + O_2$, *J. Phys. Chem., 86*, 3295-3302, 1982.

Brown, S. S., R. K. Talukdar, and A. R. Ravishankara, Reconsideration of the rate constant for the reaction of hydroxyl radicals with nitric acid, *J. Phys. Chem., 103*, 3031-3037, 1999.

Bruhl, C., P. J. Crutzen, and J. –U. Grooss, High-latitude, summertime $NO_x$ activation and seasonal ozone decline in the lower stratosphere: Model calculations based on observations by HALOE and UARS, *J. Geophys. Res., 103*, 3587-3597, 1998.

Brune, W. H., J. G. Anderson, and K. R. Chan, In situ observations of ClO over Antarctica: ER-2 aircraft results from 54°S to 72°S latitude, *J. Geophys. Res., 94*, 16,649-16,663, 1989.

Chan, K. R., S. G. Scott, T. P. Bui, S. W. Bowen, and J. Day, Temperature and horizontal wind measurements on the ER-2 aircraft during the 1987 Airborne Antarctic Ozone Experiment, *J. Geophys. Res., 94*, 11573-11587, 1989.

DeMore, W. M., et al., Chemical kinetics and photochemical data for use in stratospheric modeling, *JPL Publ., 97-4*, 1997.

Dransfield, T. J., K. K. Perkins, N. M. Donahue, J. G. Anderson, M. M. Sprengnether, and K. L. Demerjian, Temperature and pressure dependent kinetics of the gas-phase reaction of the hydroxyl radical with nitrogen dioxide, *Geophys. Res. Lett., 26*, 687-690, 1999.

Drdla, K., R. F. Pueschel, A. W. Strawa, R. C. Cohen, and T. F. Hanisco, Microphysics and chemistry of sulphate aerosols at warm stratospheric temperatures, *J. Geophys. Res.*, this issue.

Drummond, J. W., A. Volz, and D. H. Ehhalt, An optimized chemiluminescence detector for tropospheric NO measurements, *J. Atmos. Chem., 2*, 287-306, 1985.

Fahey, D. W., et al., Measurements of nitric oxide and total reactive nitrogen in the Antarctic stratosphere: Observations and chemical implications, *J. Geophys. Res., 94*, 16,665-16,681, 1989.

Gao, R. S., E. R. Keim, E. L. Woodbridge, S. J. Ciciora, M. H. Proffitt, T. L. Thompson, R. J. McLaughlin, and D. W. Fahey, New photolysis system for $NO_2$ measurements in the lower stratosphere, *J. Geophys. Res., 99*, 20,673-20,681, 1994.

Gao, R. S., et al., Partitioning of the reactive nitrogen reservoir in the lower stratosphere of the southern hemisphere: Observations and modeling, *J. Geophys. Res., 102*, 3935-3949, 1997.

Gao, R. S., B. Karcher, E. R. Keim, and D. W. Fahey, Constraining the heterogeneous loss of $O_3$ on soot particles with observations in jet engine exhaust plumes, *Geophys. Res. Lett., 25*, 3323-3326, 1998.

Gao, R. S., et al., A comparison of observations and model simulations of the $NO_x/NO_y$ ratio in the lower stratosphere, *Geophys. Res. Lett.*, in press, 1999.

Heidt, L. E., Whole air collection and analysis, *Atmos. Tech., 9*, 3-7, 1978.

Jaeglé, L., et al., In situ measurements of the $NO_2/NO$ ratio for testing atmospheric photochemical models, *Geophys. Res. Lett., 21*, 2555-2558, 1994.

Jonsson, H. H., et al., Performance of a focused cavity aerosol spectrometer for measurements in the stratosphere of particle size in the 0.06 - 2.0-μm-diameter range, *J. Atmos. Oceanic Technol., 12*, 115-129, 1995.

Kleffman, J., K. H. Becker, and P. Wiesen, Heterogeneous $NO_2$ conversion processes on acid surfaces: Possible atmospheric implications, *Atmos. Environ., 32*, 2721-2729, 1998.

Langenberg, S., V. Proksch, and U. Schurath, Solubilities and diffusion of trace gases in cold sulfuric acid films, *Atmos. Environ., 32*, 3129-3137, 1998.

Lary, D. J., A. M. Lee, R. Toumi, M. J. Newchurch, M. Pirre, and J. B. Renard, Carbon aerosols and atmospheric photochemistry, *J. Geophys. Res., 102*, 3671-3682, 1997.

Loewenstein, M., J. R. Podolske, K. R. Chan, and S. E. Strahan, Nitrous oxide as a dynamical tracer in the 1987 Airborne Antarctic Ozone Experiment, *J. Geophys. Res., 94*, 11589-11598, 1989.

McElroy, C. T., A spectroradiometer for the measurement of direct and scattered solar irradiance from on board the NASA ER-2 high-altitude research aircraft, *Geophys. Res. Lett., 22*, 1361-1364, 1995.

McElroy, C. T., C. Midwinter, D. V. Barton, and R. B. Hall, A comparison of J values from the composition and photodissociative flux measurement with model calculations, *Geophys. Res. Lett., 22*, 1365-1368, 1995.

Moonen, P. C., J. N. Cape, R. L. Storeton-West, and R. McColm, Measurement of the NO + $O_3$ reaction rate at atmospheric pressure using realistic mixing ratios, *J. Atmos. Chem., 29*, 299-314, 1998.

Osterman, G. B., et al., The budget and partitioning of reactive nitrogen species in the Arctic stratosphere, *Geophys. Res. Lett., 26*, 1157-1160, 1999.

Prather, M. J., Ozone in the upper stratosphere and mesosphere, *J. Geophys. Res., 86*, 5325-5338, 1981.

Proffitt, M. H., et al., In situ ozone measurements within the 1987 Antarctic ozone hole from a high-altitude ER-2 aircraft, *J. Geophys. Res., 94*, 16,547-16,556, 1989.

Randeniya, L. K., P. F. Vohralik, I. C. Plumb, and K. R. Ryan, Heterogeneous $BrONO_2$ hydrolysis: Effect on $NO_2$ columns and ozone at high latitudes in summer, *J. Geophys. Res., 102*, 23,543-23,557, 1997.

Rogaski, C. A., D. M. Golden, and L. R. Williams, Reactive uptake and hydration experiments on amorphous carbon treated with $NO_2$, $SO_2$, $O_3$, $HNO_3$, and $H_2SO_4$, *Geophys. Res. Lett., 24*, 381-384, 1997.

Salawitch, R. J., et al., The distribution of hydrogen, nitrogen, and chlorine radicals in the lower stratosphere: Implications for changes in $O_3$ due to emission of $NO_y$ from supersonic aircraft, *Geophys. Res. Lett., 21*, 2547-2550, 1994a.

Salawitch, R. J., et al., The diurnal variation of hydrogen, nitrogen, and chlorine radicals: Implications for the heterogeneous production of $HNO_2$, *Geophys. Res. Lett., 21*, 2551-2554, 1994b.

Sen, B., G. C. Toon, G. B. Osterman, J.-F. Blavier, J. J. Margitan, R. J. Salawitch, and G. K. Yue, Measurements of reactive nitrogen in the stratosphere, *J. Geophys. Res., 103*, 3571-3585, 1998.

Tabor, K., L. Gutzwiller, and M. J. Rossi, Heterogeneous chemical kinetics of $NO_2$ on amorphous carbon at ambient temperature, *J. Phys. Chem., 98*, 6172-6186, 1994.

Wamsley, P. R., et al., Distribution of halon-1211 in the upper troposphere and lower stratosphere and the 1994 total bromine budget, *J. Geophys. Res., 103*, 1513-1526, 1998.

Wennberg, P. O., et al., Removal of stratospheric $O_3$ by radicals: In situ measurements of OH, $HO_2$, NO, $NO_2$, ClO, and BrO, *Science, 266*, 398-404, 1994.

Wennberg, P. O., T. F. Hanisco, R. C. Cohen, R. M. Stimpfle, L. B. Lapson, and J. G. Anderson, In situ measurements of OH and $HO_2$ in the upper troposphere and stratosphere, *J. Atmos. Sci., 52*, 3413-3420, 1995.

Wennberg, P. O., et al., Twilight observations suggest unknown sources of $HO_x$, *Geophys. Res. Lett., 26*, 1373-1376, 1999.

Woodbridge, E. L., et al., Estimates of total organic and inorganic chlorine in the lower stratosphere from in situ and flask measurements during AASE II, *J. Geophys. Res., 100*, 3057-3064, 1995.

D. E. Anderson, T. L. Kusterer, and S. A. Lloyd, Applied Physics Laboratory, Atmospheric Remote Sensing Group, The Johns Hopkins University, Laurel, MD 20723.

G. P. Bonne, K. K. Perkins, R. M. Stimpfle, and P. B. Voss, Department of Chemistry, Harvard University, Cambridge, MA 02138.

T. P. Bui, NASA Ames Research Center, Moffett Field, CA 94035.

R. C. Cohen and L. C. Koch, Department of Chemistry, UC Berkeley, Berkeley, CA 94720.

L. A. Del Negro (corresponding author), NOAA Climate Monitoring and Diagnostics Laboratory, 325 Broadway R/E/CG1, Boulder, CO 80303. (ldelnegro @cmdl.noaa.gov)

S. G. Donnelly, R. S. Gao, J. A. Neuman, and M. H. Proffitt, NOAA Aeronomy Laboratory and Cooperative Institute for Research in Environmental Sciences, University of Colorado, Boulder, CO 80309.

D. W. Fahey, NOAA Aeronomy Laboratory, 325 Broadway R/E/AL6, Boulder, CO, 80303.

E. R. Keim, Space and Environmental Technology Center, The Aerospace Corporation, Los Angeles, CA 90009.

L. R. Lait, NASA Goddard Space Flight Center, Greenbelt, MD 20771.

J. Margitan and R. J. Salawitch, Jet Propulsion Laboratory, California Institute of Technology, Pasadena, CA 91109.

C. T. McElroy, Atmospheric Environment Service/Environment Canada, Downsview, Ontario, Canada M3H 5T4.

W. H. Swartz, Department of Chemistry and Biochemistry, University of MD, College Park, Maryland 20742.

P. O. Wennberg, Division of Geological and Planetary Sciences, California Institute of Technology, Pasadena, CA 91125.

(Received December 4, 1998; revised April 8, 1999;
accepted April 13, 1999.)